The Cullin-3–Rbx1–KCTD10 complex controls endothelial barrier function via K63 ubiquitination of RhoB

Igor Kovačević,[1,2]* Tomohisa Sakaue,[3,4,5]* Jisca Majoleé,[1] Manon C. Pronk,[2] Masashi Maekawa,[3,5] Dirk Geerts,[6] Mar Fernandez-Borja,[1] Shigeki Higashiyama,[3,5] and Peter L. Hordijk[2]

[1]Department of Molecular Cell Biology, Sanquin Research, Amsterdam, Netherlands
[2]Department of Physiology, Vrije Universiteit University Medical Center, Amsterdam, Netherlands
[3]Division of Cell Growth and Tumor Regulation, Proteo-Science Center, Ehime University, Toon, Ehime, Japan
[4]Department of Cardiovascular and Thoracic Surgery and [5]Department of Biochemistry and Molecular Genetics, Ehime University Graduate School of Medicine, Toon, Ehime, Japan
[6]Department of Pediatric Oncology/Hematology, Erasmus University Medical Center, Rotterdam, Netherlands

RhoGTPases control endothelial cell (EC) migration, adhesion, and barrier formation. Whereas the relevance of RhoA for endothelial barrier function is widely accepted, the role of the RhoA homologue RhoB is poorly defined. RhoB and RhoA are 85% identical, but RhoB's subcellular localization and half-life are uniquely different. Here, we studied the role of ubiquitination for the function and stability of RhoB in primary human ECs. We show that the K63 polyubiquitination at lysine 162 and 181 of RhoB targets the protein to lysosomes. Moreover, we identified the RING E3 ligase complex Cullin-3–Rbx1–KCTD10 as key modulator of endothelial barrier integrity via its regulation of the ubiquitination, localization, and activity of RhoB. In conclusion, our data show that ubiquitination controls the subcellular localization and lysosomal degradation of RhoB and thereby regulates the stability of the endothelial barrier through control of RhoB-mediated EC contraction.

Introduction

Endothelial cells (ECs) are tightly connected cells that line the luminal side of blood and lymphatic vessels. Loss of endothelial barrier integrity is a hallmark of chronic inflammatory diseases and will lead to edema, tissue damage, and loss of organ function. Adherens junctions (AJs) are key structures in the regulation of endothelial barrier function (Dejana et al., 1999). AJ-associated protein complexes form contacts between two neighboring ECs through Ca^{2+}-dependent, homotypic interaction of vascular endothelial (VE)–cadherin molecules. The interaction of the VE–cadherin complex with the actin cytoskeleton limits its endocytosis and stabilizes AJs (Hirano et al., 1992). Conversely, altered actin dynamics can induce junctional rearrangement and contractility-driven disassembly of AJs (Hordijk et al., 1999).

Morphology and dynamics of the actin cytoskeleton are regulated at the level of actin (de)polymerization as well as bundling and the interaction of polymerized actin with the cell adhesion machinery, processes regulated by Rho GTPases. For example, activation of Rac1 or Cdc42 induces actin polymerization and formation of membrane protrusions, which promote cell migration (Nobes and Hall, 1995). In contrast, activation of RhoA induces myosin activation, F-actin stress fiber formation, and cell contraction. In ECs, the latter pathway promotes force-induced disassembly of AJs and loss of endothelial integrity (Essler et al., 2000; van Nieuw Amerongen et al., 2000; Verin et al., 2001; Vouret-Craviari et al., 2002).

Given the pathophysiological relevance of endothelial integrity, it is crucial to uncover the molecular details of the mechanisms that drive RhoGTPase (in)activation. After initial studies (Ridley et al., 1992; Ridley and Hall, 1992), analysis of regulation of Rho GTPases has led to the discovery of guanine nucleotide exchange factors, GTPase-activating proteins, and guanine nucleotide dissociation inhibitors that govern the activation, inactivation, and the stability of Rho GTPases, respectively (Cherfils and Zeghouf, 2013).

Posttranslational modifications such as ubiquitination were also found to control the localization, activity, and stability of Rho GTPases, including RhoA and Rac1 (Chen et al., 2009, 2011; Nethe et al., 2010; Torrino et al., 2011; Schaefer et al., 2014). Ubiquitination involves covalent attachment of an ubiquitin moiety to a lysine residue in the substrate (de Bie and

---

*I. Kovačević and T. Sakaue contributed equally to this paper.
Correspondence to Peter L. Hordijk: p.hordijk@vumc.nl; Shigeki Higashiyama: shigeki@m.ehime-u.ac.jp

Ciechanover, 2011). Several inhibitors of the ubiquitination machinery are currently tested in clinical trials for treatment of solid tumors and leukemia (e.g., MLN4924; Zhang and Sidhu, 2014).

Currently, the molecular mechanism that links ubiquitination to GTPase-regulated endothelial integrity is unknown. We therefore tested whether inhibition of ubiquitination using a targeted shRNA-mediated knockdown approach would affect endothelial barrier stability. Based on published information (Wang et al., 2006; Chen et al., 2009; Oberoi et al., 2012; Yang et al., 2013b; Zhao et al., 2013), we selected ubiquitination-regulating enzymes and associated proteins that might target Rho GTPases for degradation in ECs. We found that depletion of members of Cullin–RING ligase (CRL) family of proteins, specifically Cullin-3, strongly impairs endothelial barrier function. Furthermore, we found that loss of Cullin-3 selectively impairs RhoB degradation and that CRL inhibition by MLN4924 increases RhoB levels and activation. In addition, we found that RhoB is primarily K63 polyubiquitinated and subsequently degraded in lysosomes. Using a focused siRNA screen, we identified the BTB protein KCTD10 as substrate receptor for RhoB in the Cullin-3–Rbx1 ligase complex. Finally, we identified at least two lysine residues of RhoB, K162 and K181, as acceptor residues for KCTD10-mediated ubiquitination.

Our results show that continuous, Cullin-3–Rbx1–KCTD10–mediated RhoB ubiquitination and degradation preserves endothelial barrier function, supporting the concept that controlled protein turnover in ECs is instrumental for the maintenance of blood vessel integrity.

Results

Ubiquitination regulates the actin cytoskeleton and AJs in ECs

Activity of RhoGTPases is crucial for actin dynamics and endothelial barrier function (van Nieuw Amerongen et al., 2007; Timmerman et al., 2015). Therefore, we hypothesized that interfering with ubiquitination of Rho GTPases would impact F-actin distribution and endothelial integrity. To test this, we used lentiviral shRNA-mediated knockdown of 22 genes (Fig. S1, A and B) comprising E3 ubiquitin ligases, CRL substrate recognition receptors, ubiquitin proteases, and other proteins and analyzed the consequences for the actin cytoskeleton and AJ morphology (Fig. S1, B and C).

In line with published data, we found an increase of actin stress fibers when we depleted XIAP, BIRC2 (Rac1 ubiquitin ligases), or SMURF1 (a RhoA ubiquitin ligase; Fig. S1 B; Wang et al., 2006; Oberoi et al., 2012). Interestingly, depletion of CRL complex proteins (Cullin-3, FBXW7, and FBXL19; Fig. S1 B) strongly affected the actin cytoskeleton and VE–cadherin distribution (see following paragraph). Based on these initial and published observations (Chen et al., 2009), we focused on the role of Cullin-3 in cytoskeletal organization and endothelial barrier function.

Cullin-3 is crucial for maintenance of endothelial barrier integrity

Depletion of Cullin-3 led to increased formation of F-actin stress fibers in primary human umbilical vein endothelial cells (HUVECs; Figs. 1 A and S1 D) and an ~20% decrease in transendothelial electrical resistance (Fig. 1, B and C). Using multifrequency scanning and modeling software, we found that Cullin-3 knockdown decreased Rb (barrier resistance) ~10-fold (Fig. 1 D).

Thrombin-induced disruption of the endothelial barrier is used to define the role of GTPases, kinases, and phosphatases in vascular integrity (Beckers et al., 2010; Reinhard et al., 2016). The modulation of endothelial integrity by Thrombin, histamine, or sphingosine-1-phoshate (S1P), occurs through G-protein–coupled receptors (Coughlin, 1999; Ozaki et al., 2003). This ensures rapid, but also transient responses, in contrast to the barrier loss induced by inflammatory cytokines such as TNFα or growth factors such as VEGF (Amado-Azevedo et al., 2014; Clark et al., 2015). The Thrombin-induced loss of endothelial resistance (Fig. 1 E) was not altered by Cullin-3 depletion (Fig. 1, E and F). However, the subsequent recovery of endothelial barrier function was significantly impaired (Fig. 1 G), suggesting that Cullin-3 protects against Thrombin-induced, prolonged loss of integrity in ECs.

To test whether barrier-promoting signaling was affected in Cullin-3 knockdown cells, we treated ECs with S1P (Fig. 1 E). We did not observe any significant change in the barrier-protecting response to S1P upon loss of Cullin-3 measured at 4,000 Hz (Fig. 1 H). However, depletion of Cullin-3 caused a three- to fourfold increase in resistance when measured at 32,000 Hz (Fig. 1 I). These data suggest that loss of Cullin-3 promotes barrier function through increased cell–matrix interactions.

Cullin-3 depletion impairs FA dynamics in ECs

Adhesion of ECs to the extracellular matrix is mediated by integrins. We found that α5 integrin– and activated-β1-integrin–positive adhesions were increased in size in S1P-stimulated, Cullin-3 knockdown cells (Fig. 2 A). Based on the immunofluorescence (Figs. 1 A and 2 A) and electrical cell-impedance sensing (ECIS) data (Fig. 1, B–D), we concluded that the increased adhesion and integrin activation in Cullin-3 knockdown cells was caused by increased contractility. In line with this, we found that depletion of Cullin-3 increased the phosphorylation status of Erk1/2 5.2-fold (Fig. 2, B and C) and of myosin light chain (MLC) 6.5-fold (Fig. 2, B and D), but not that of PAK1/2/3 (Fig. 2 B). As shown in Fig. 1 A, Cullin-3 depletion induces formation of actin stress fibers, anchored at focal adhesions (FAs). Staining for phospho Paxillin (pPaxillin) and vinculin, well-established FA markers, showed a shift in distribution of FA from the cell periphery in control cells to a more central distribution in Cullin-3 knockdown cells (Fig. S2 A). Subsequent live-cell microscopy (Fig. 2 E and Videos 1 and 2) showed that depletion of Cullin-3 leads to an increased assembly rate of FAs (Fig. 2 F), whereas FA disassembly was not affected (Fig. 2 G). Thus, Cullin-3 attenuates both MLC phosphorylation and FA assembly rate in ECs.

Chemical inhibition of CRLs by MLN4924 causes loss of endothelial barrier integrity and induces FA formation

CRLs are activated by covalent attachment of the ubiquitin-like protein Nedd8 to the Cullin subunit. MLN4924 (Pevonedistat) inhibits the Nedd8-activating enzyme, blocking CRL activation (Soucy et al., 2009). In line with the findings described in the previous paragraph, we found that MLN4924 increased formation of FAs threefold (Fig. 2, H and I) with only a modest increase in FA size (Fig. 2, H and J). Additionally, we found that MLN4924 increased formation of stress fibers and cortical actin
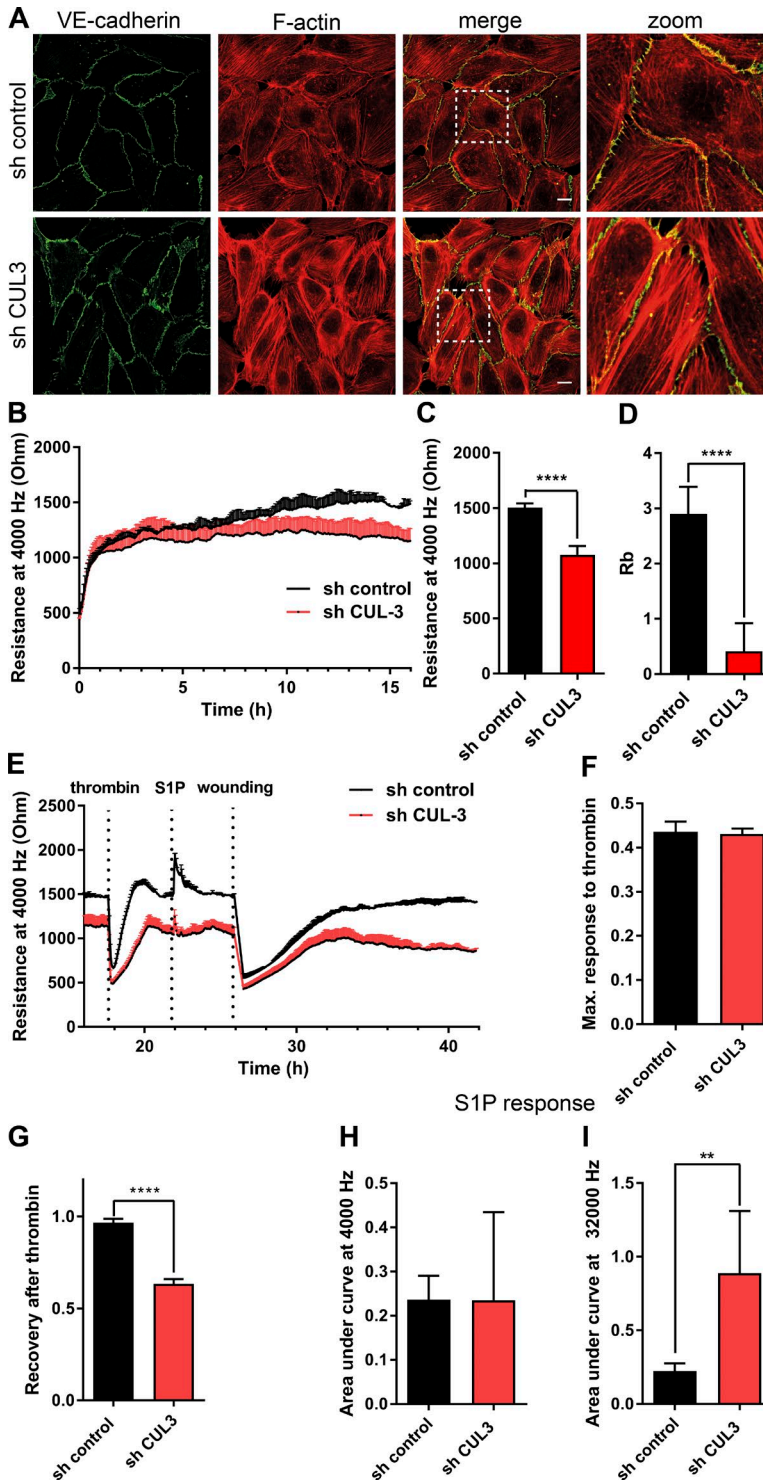
Figure 1. **Knockdown of Cullin-3 impairs cell signaling involved in endothelial barrier maintenance. (A)** HUVECs were transduced with the control shRNA or Cullin-3–targeting shRNA and stained for VE–cadherin and F-actin at 72 h after infection. Dashed boxes correspond to zoomed images. Bars, 15 µm. **(B)** ECIS measurement of HUVECs prepared as in A. 10^5 cells were seeded per well in an eight-well ECIS slide at 72 h after infection, and electrical resistance was measured at 4,000 Hz ($n = 5$). **(C)** Resistance values at 4,000 Hz were compared by analysis of 10 measurement points 16–17 h after seeding for the cells prepared as in A ($n = 5$). **(D)** Quantification of the Rb parameter was analyzed as in C. **(E)** HUVECs were prepared as in A, and the resistance of the endothelial monolayer was measured at 4,000 Hz using ECIS. Cells were stimulated with 1 U/ml thrombin and, after recovery, with 500 nM S1P, and electrical wounding was performed at 100 kHZ, 6,500 µA for 120 s. **(F)** Maximum response to thrombin response was calculated using GraphPad Prism ($n = 5$). **(G)** Recovery upon thrombin stimulation was measured at 1.5 h upon thrombin addition and normalized to the resistance values before thrombin addition ($n = 5$). **(H and I)** Analysis of S1P response in cells prepared as in A ($n = 5$). Areas under the curve of S1P response were calculated using GraphPad Prism. Error bars represent SD. **, P = 0.01–0.001; ****, P < 0.0001.

bundles (Fig. 3 A), accompanied by contraction and formation of intercellular gaps.

Disruption of endothelial integrity by MLN4924 was further confirmed by ECIS analysis (Fig. 3 B). The gradual loss of endothelial resistance induced by MLN4924 surpassed the effect induced by the inflammatory cytokine TNF-α (Fig. 3 B), with no additive effect of combining TNF-α with MLN4924. MLN4924 also induced a loss of junctional VE–cadherin staining (Fig. S2 B). These data show that CRL activity, specifically Cullin-3, is important for the maintenance

of the endothelial barrier through the regulation of AJ stability and FA formation.

CRL inhibition disrupts endothelial barrier via stabilization and activation of RhoB

It was previously reported that MLN4924 inhibits degradation of RhoB in liver cancer and ECs (Xu et al., 2015). Therefore, we tested whether the MLN4924-induced contraction and loss of barrier integrity (Fig. 3, A and B) was caused by its effects on RhoB. RhoB, but not Rac1 or RhoC, levels in HUVECs were
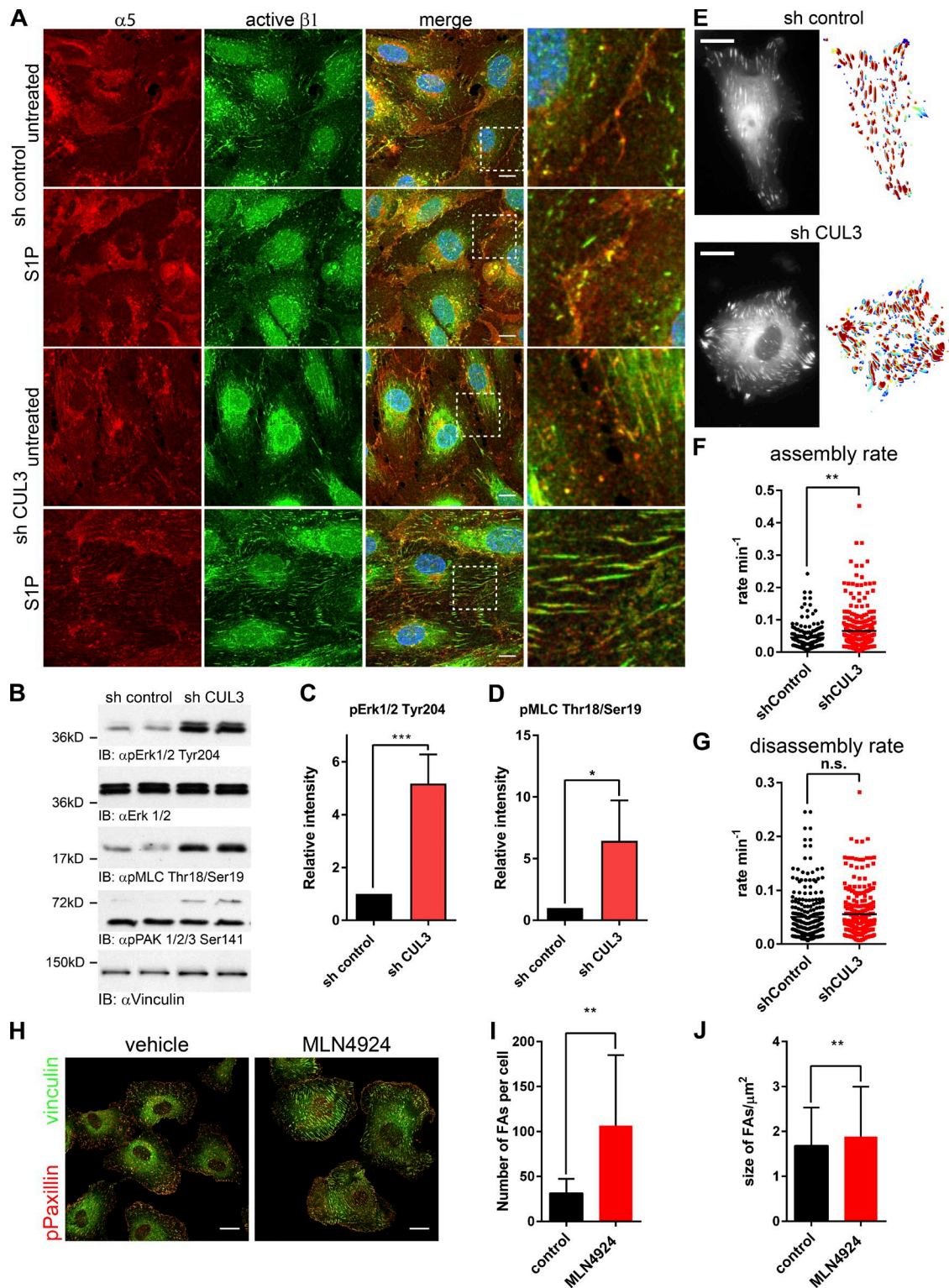
Figure 2. **Cullin-3 knockdown and MLN4924 treatment impair FA dynamics in ECs. (A)** Immunofluorescence staining of HUVECs transduced with the control- or Cullin-3 shRNA and stimulated with 500 nM SP1 for 15 min. Upon stimulation, cells were fixed and stained for α5- and activated β1-integrin. Bars, 10 μm. Higher magnifications of marked regions are in the right panels. **(B)** Immunoblots (IB) of duplicate lysates prepared from HUVECs transduced with the control shRNA or Cullin-3 shRNA. Membranes were probed with pErk Tyr204, pMLC Thr18/Ser19, and pPAK 1/2/3 Ser141 antibodies. Erk1/2 and vinculin were used as loading control. **(C and D)** Densitometric analysis of the pErk1/2 Tyr204 (C) and pMLC Thr18/Ser19 (D) immunoblots (n = 5). **(E)** Still images of movies (Videos 1 and 2) of control and CUL3 shRNA-transduced HUVECs, cotransfected with GFP-vinculin. Bars, 15 μm. On the right side of the respective image, an overlay of all adhesions is shown. Blue, FAs at the earliest time points; red, FAs at the latest time points. **(F and G)** Assembly rate (F) and disassembly rate (G) were obtained from analysis of single adhesions via the FA analysis server (http://faas.bme.unc.edu/). **(H)** Confocal immunofluorescence of HUVECs treated with 500 nM MLN4924 for 4 h. After stimulation, cells were fixed and stained for pPaxillin and vinculin. Bars, 20 μm. **(I and J)** The number of FAs per cell (I) and the mean size of FAs (J) were analyzed using ImageJ software and the particle analysis function. All adhesions in the range of 1–10 μm² from 10 cells per condition were included in the analysis. Error bars represent SD. n.s., P ≥ 0.05; *, P = 0.01–0.05; **, P = 0.01–0.001; ***, P = 0.001–0.0001.
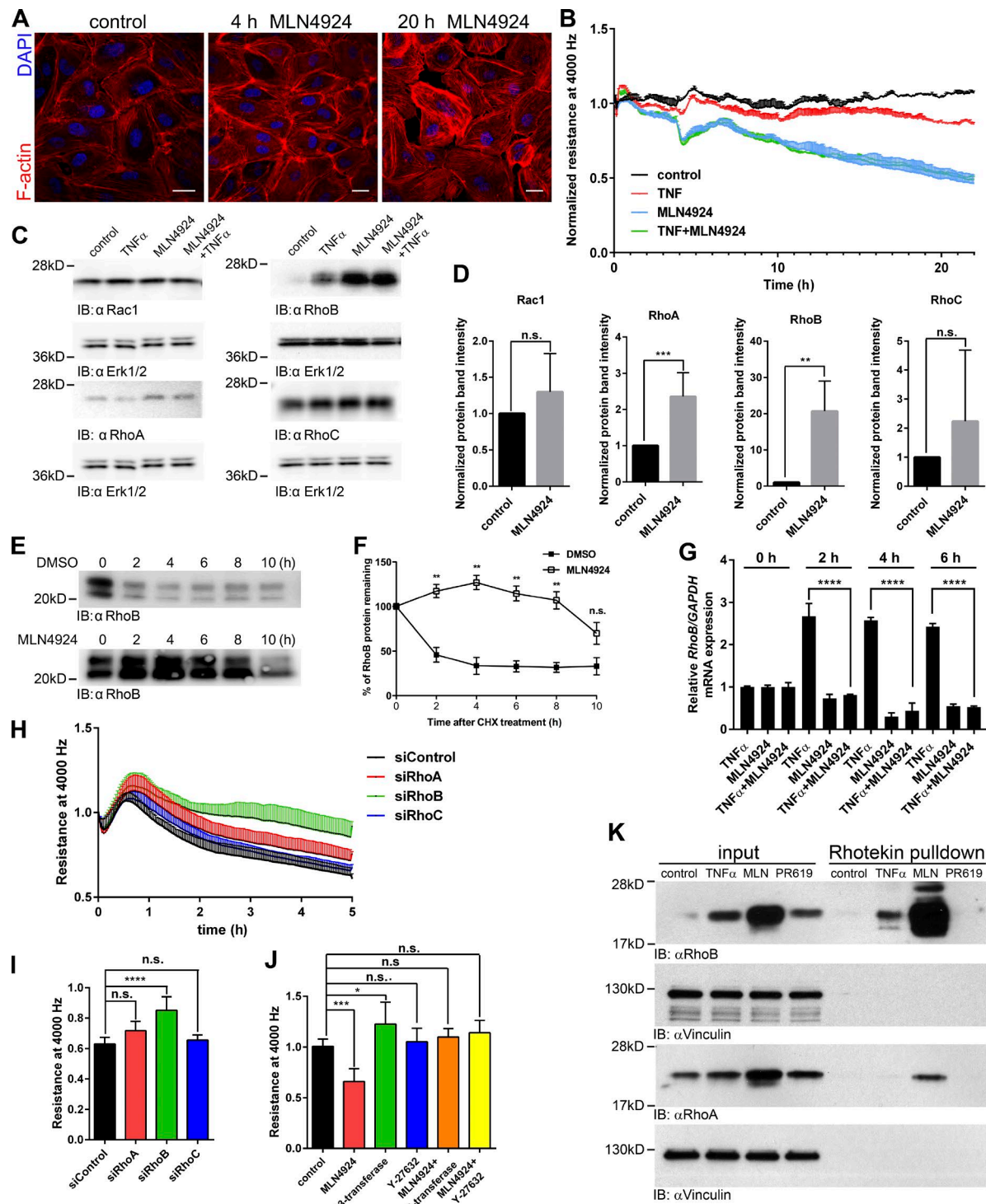
Figure 3. **MLN4924 treatment increases expression, and activation of RhoB and disrupts the endothelial barrier. (A)** The F-actin network in HUVECs treated with 500 nM MLN4924 for 4 and 20 h. Bars, 20 µm. **(B)** ECIS measurement of a HUVEC monolayer treated with 500 nM MLN4924, 10 ng/ml human TNF-α, or both. Resistance at 4,000 Hz was measured, and the graph shows a representative experiment with triplicate measurements per condition. **(C)** Immunoblot analysis of Rho GTPases in HUVECs treated with 500 nM MLN4924, 10 ng/ml human TNF-α, or both for 4 h. Lysates were probed with Rac1, RhoA, RhoB, and RhoC antibodies; Erk1/2 was included as loading control. Erk1/2 loading control is identical for Rac1 and RhoA immunoblots. **(D)** Densitometric analysis of Rac1, RhoA, RhoB, and RhoC immunoblots. Rac1, RhoA, RhoB, and RhoC expression was normalized to the loading control and in MLN4924-treated samples normalized to the corresponding untreated controls ($n = 3–7$). **(E)** Effect of MLN4924 on RhoB protein stability. HUVECs were pretreated with 500 nM MLN4924 or DMSO control for 48 h followed by addition of 25 µg/ml cycloheximide for the indicated time points. Cells were lysed, and 20 µg of total proteins was analyzed by immunoblot with anti–RhoB antibody. **(F)** Densitometric analysis of E was performed using ImageJ software ($n = 3$). **(G)** RT-PCR analysis of RhoB mRNA expression in HUVECs treated with 500 nM MLN4924, 10 ng/ml human TNF-α, or both for indicated times. mRNA was isolated upon treatment and analyzed for RhoB transcripts using RT-PCR ($n = 3$). **(H)** HUVECs were transfected with siRNA targeting RhoA, RhoB, RhoC, or control siRNA. 72 h after transfection, cells were starved for 24 h and treated with 500 nM MLN4924, after which resistance was measured at 4,000 Hz and normalized to values before the addition of MLN4924. **(I)** Quantification of H at 5 h after addition of MLN4924 ($n = 7$).

increased 20-fold upon 4 h of MLN4924 treatment (Fig. 3 C and D). RhoA showed a modest, MLN4924-induced increase in expression (3.5-fold; Fig. 3, C and D). In cycloheximide-chase experiments, we found that the effects of MLN4924 on RhoB and RhoA were caused by increased protein stability (Fig. 3, E and F; and Fig. S2 C) and not increased de novo protein synthesis (Fig. 3 G).

TNF-α increased expression of RhoB as well (Kroon et al., 2013; Fig. 3 C). Quantitative PCR analysis showed that TNF-α efficiently induced transcription of RhoB mRNA after 2 h (Fig. 3 G). In line with this, inhibition of protein synthesis with cycloheximide completely abrogated TNF-α–induced RhoB expression (Fig. S2 D). We next depleted RhoA/B/C proteins individually or in combination (Fig. S4 A). We found that transendothelial resistance in control cells, treated with MLN4924, dropped to 60% after 5 h and that depletion of RhoB, but not RhoA or RhoC, rescued this loss of resistance (Fig. 3, H and I). The combined knockdown of RhoA and RhoB and of RhoA/B/C was very efficient in rescuing the effect induced by MLN4924 (Fig. S3, B and C). This was further confirmed using the cell-permeable C3 transferase, which inactivates all three Rho GTPases (Figs. 3 J and S3 D). Finally, inhibition of the Rho-effector kinases ROCK1/2 (Amado-Azevedo et al., 2014) with Y27632 before MLN4924 treatment prevented the loss of endothelial monolayer resistance (Figs. 3 J and S3 D). These results show that protection of endothelial monolayer integrity by CRL is largely mediated via ubiquitination and degradation of RhoB, which signals through ROCK to induce EC contraction.

Next, we tested whether the increased expression of RhoB in MLN4924- or TNF-α–treated HUVECs was accompanied by increased RhoB activity. Using a Rhotekin-RBD pull-down assay, we could show that MLN4924 caused a strong activation of RhoB and, to a lesser extent, RhoA (Fig. 3 K), but not Rac1 (Fig. S4 E), whereas a 4-h TNF-α stimulation induced only minor activation of RhoB.

In contrast to inhibition of CRL, the deubiquitination inhibitor PR619 did not alter RhoB activation and induced only a minor increase in RhoB expression (Fig. 3 K). However, PR619 decreased the levels and activity of Rac1, in line with published data (Lerm et al., 2002).

Ubiquitination targets RhoB to lysosomes in ECs

We next tested whether RhoB ubiquitination regulates its localization. TNF-α–induced RhoB is primarily localized in the endosomal compartment (Fig. 4, A and B), in particular in lysosomes (Fig. 4, C and D). In marked contrast, MLN4924-induced RhoB was primarily localized at the cell membrane (Fig. 4, A and B). If MLN4924 was added together with TNF-α, we observed the same increase in RhoB expression as with TNF-α, but this pool of RhoB failed to localize to the endosomal compartment (Fig. 4, A–D).

Because of its localization in lysosomes, we hypothesized that RhoB is degraded via the lysosomal and proteasomal pathways. We found that inhibitors of lysosomal acidification (chloroquine and NH_4Cl) or an inhibitor of lysosomal proteases

(leupeptin) increased RhoB expression, similar to the proteasome inhibitors bortezomib or MG132 and MLN4924 (Fig. 4, D and E; and Fig. S3 F). In addition, inhibition of the proteasome or, even more efficiently, lysosomal inhibition both led to accumulation of RhoB in lysosomes, specifically in LAMP-1–positive lysosomal membranes (Fig. 4, F and G). Although some of these inhibitors, such as chloroquine and NH_4Cl, have limited specificity, these data suggest that RhoB ubiquitination promotes its localization to lysosomes and that RhoB degradation occurs through a lysosomal as well as a proteasomal pathway.

RhoB is polyubiquitinated via K63 linkage at lysines 162 and 181

Immunoprecipitation of endogenous RhoB from HUVECs confirmed that RhoB is polyubiquitinated under normal conditions and that this was completely prevented by MLN4924-mediated inhibition of CRLs (Fig. 5 A). Conversely, inhibition of deubiquitination by PR619 increased the levels of polyubiquitinated RhoB (Fig. 5 A). TNF-α did not reduce ubiquitination of endogenous (Fig. 5 A) or transfected RhoB (Fig. S4 A). Immunofluorescence analysis showed that RhoB colocalized with K63-polyubiquitin chains in endosomes in a CRL-dependent fashion (Fig. 5 B). These data suggest that RhoB might be K63 ubiquitinated followed by translocation to, and degradation in, lysosomes. Using an in vivo ubiquitination assay, we found that RhoB T19N is predominantly polyubiquitinated by K63-linked ubiquitin chains and that this was inhibited by MLN4924 (Fig. 5 C). Based on published data, we hypothesized that the lysine acceptor site for RhoB ubiquitination is close to the C terminus (Lebowitz et al., 1995; Michaelson et al., 2001). Therefore, we mutated lysines, the side chains of which are exposed on the surface of the RhoB structure (Fig. 5 D). Although mutation of lysine 135 did not interfere with K63 polyubiquitination of RhoB, mutation of either lysine 162 or 181 almost completely abolished K63 polyubiquitination of RhoB (Fig. 5 E). In the next experiment, we transfected wild-type or the K162/181R double mutant of RhoB in ECs and analyzed the effects on cell size as a measure for contraction. Wild-type RhoB decreased cell size by 50%, whereas the K161/181R double mutant of RhoB induced even stronger contraction and a 60% reduction in cell size (Fig. 5 F). Moreover, ECIS measurements showed that the K162/181R mutant of RhoB significantly decreased endothelial monolayer resistance (Fig. 5 G). Finally, we found that lysosomal inhibition increased wild-type, transfected RhoB by 40%, whereas expression of the K162/181R mutant was not increased (Fig. 5, H and I). Thus, we conclude that CRL-mediated polyubiquitination of RhoB is primarily K63 linked and occurs at two lysine residues (K162 and K181), which allows lysosomal degradation.

Cullin-3 is required for RhoB degradation in ECs

Knockdown of Cullin-3 in ECs induced robust expression of RhoB (Fig. 6, A and B). To test for a specific role of Cullin-3 in the degradation of RhoB, we knocked down Cullin-1, Cullin-2, and Cullin-3 in HUVECs and analyzed RhoB expression. As a

---

(J) Quantification of the MLN4924 effect on the barrier function of HUVECs pretreated with Y-27632 or C3-transferase. Graph represents normalized resistance at 15 h after MLN4924 addition ($n = 3$–8). (K) Rhotekin pull-downs were performed using lysates of HUVECs treated or not with 500 nM MLN4924 or 10 ng/ml human TNF-α for 4 h or with 2.5 µM PR619 for 2 h. Input is equal to 2.5% of the lysate used for the pull-down. Vinculin was used as loading control ($n = 3$). Error bars represent SD. n.s., $P \geq 0.05$; *, $P = 0.01$–0.05; **, $P = 0.01$–0.001; ***, $P = 0.001$–0.0001; ****, $P < 0.0001$.
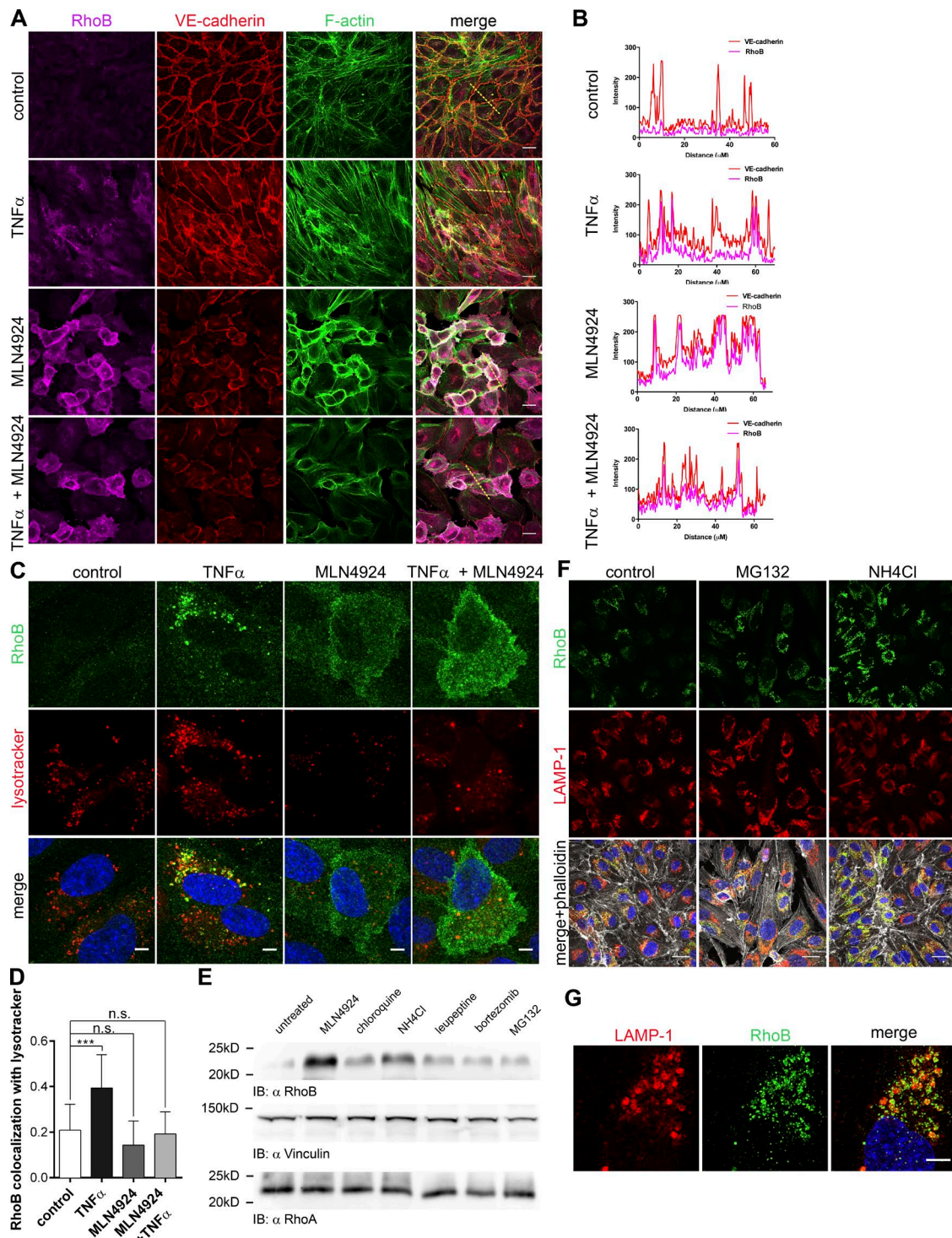
Figure 4. **CRL-mediated ubiquitination targets RhoB for lysosomal degradation in ECs.** **(A)** HUVECs were treated overnight with 300 nM MLN4924, 10 ng/ml human TNF-α, or a combination of both. Cells were fixed and stained for RhoB and VE–cadherin, F-actin, and nuclei. Bars, 20 µm. **(B)** Line scans of fluorescence intensity of RhoB and VE–cadherin were performed on images shown in A and analyzed using ImageJ. Yellow dashed lines in A mark the scanned area. **(C)** Colocalization of RhoB with Lysotracker in TNF-α–treated HUVECs. Cells were treated and stained as in A. Before fixation, cells were incubated with Lysotracker for 30 min. Bars, 5 µm. **(D)** Quantification of Mander's coefficient of colocalization of RhoB colocalization with Lysotracker was performed using ImageJ and JACoP plugin (Bolte and Cordelières, 2006; n = 17–19). **(E)** Immunoblot (IB) analysis of the RhoA and RhoB expression in HUVECs treated for 4 h with 500 nM MLN4924, 20 nM bortezomib, 5 µM MG132, 100 µM chloroquine, 30 mM NH4Cl, or 50 µM leupeptin. Vinculin was included as loading control. **(F)** Immunofluorescence staining of HUVECs treated overnight with 5 µM MG132 or 10 mM NH4Cl. After treatment, cells were fixed and stained with RhoB and LAMP-1 antibodies and phalloidin. Bars, 20 µM. **(G)** Samples for confocal microscopy were prepared as in F with MG132 treatment. Images were captured using a Leica TCS SP8 X (Leica Microsystems) microscope using a 100× 1.4 NA oil objective. Images were acquired at Nyquist rate using Nyquist Calculator (Scientific Volume Imaging) and subsequently deconvolved using Huygens Professional (Scientific Volume Imaging). Dashed box represents an enlarged lysosome, which is depicted in upper left corner of each panel. Bar, 5 µm. Error bars represent SD. n.s., P ≥ 0.05; ***, P = 0.001–0.0001.
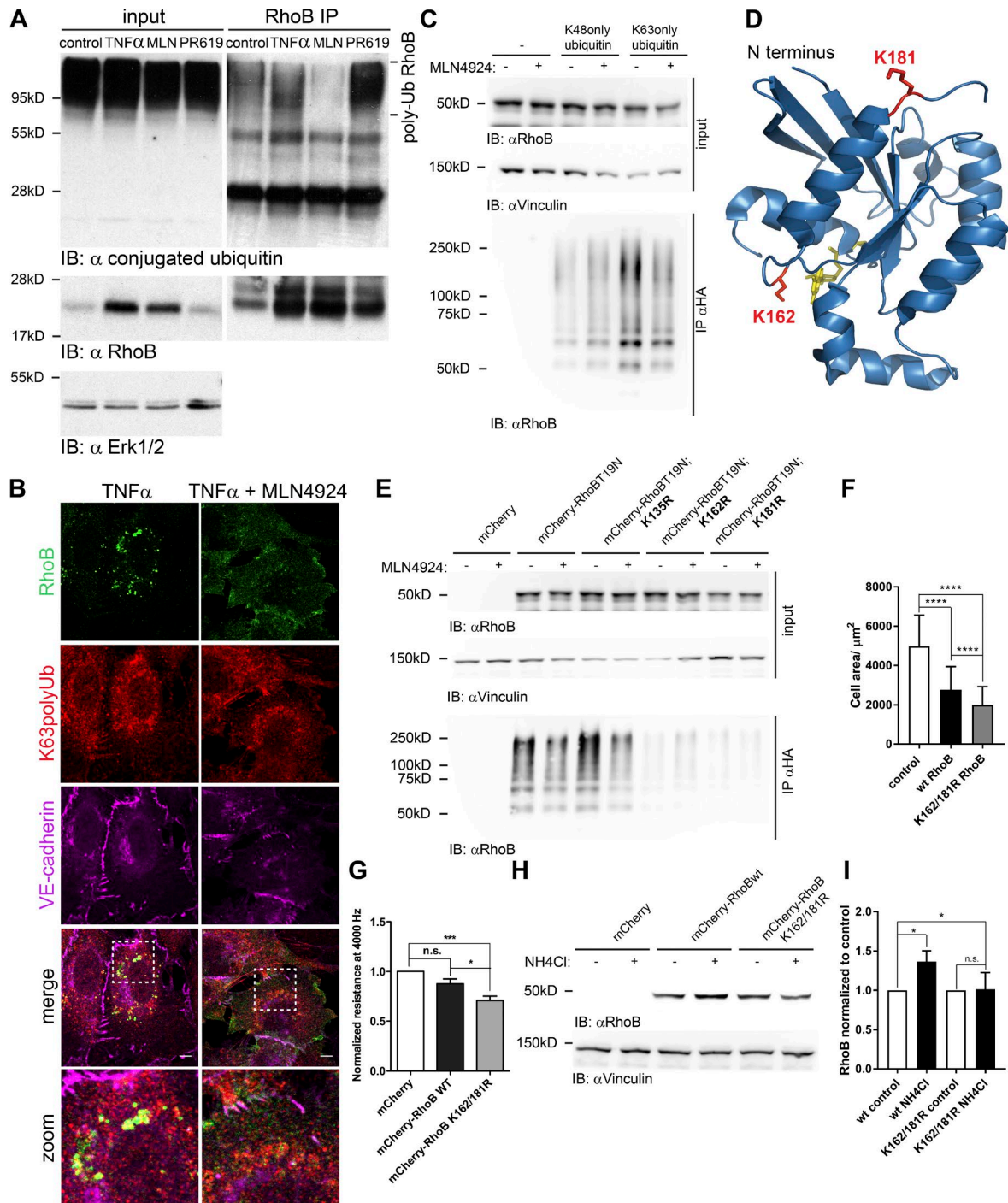
Figure 5. **RhoB is K63 polyubiquitinated by CRLs on lysines 162 and 181.** **(A)** RhoB was immunoprecipitated (IP) from lysates of HUVECs treated with MLN4924, TNF-α, or PR619. Input is equal to 2.5% of the lysate used for immunoprecipitation. Ubiquitinated proteins were detected using ubiquitin (Ub; FK-2) antibody. Polyubiquitinated RhoB is indicated on the right. **(B)** Confocal immunofluorescence staining of RhoB in HUVECs treated with 10 ng/ml TNF-α or 10 ng/ml TNF-α in combination with 300 nM MLN4924. Cells were stained for RhoB, polyubiquitin K63, and VE–cadherin. Zoomed areas (white boxes) are shown at the bottom. Bars, 10 µm. **(C)** Denaturing coimmunoprecipitation of ubiquitin and RhoB. HEK293T cells were cotransfected with HA-ubiquitin K48 only or HA-ubiquitin K63 only and mCherry-RhoB-T19N. Samples were analyzed by immunoblotting for presence of RhoB using RhoB antibody. Vinculin immunoblot was used as a control. **(D)** 3D structure of RhoB and indication of lysines 162 and 181. Ribbon structure of RhoB (aa 4–187) was obtained from the Protein Data Bank (2FV8). The figure was prepared using Pymol molecular visualization system (Schrödinger). Lysine residues 162 and 181 are shown in red. **(E)** Denaturing coimmunoprecipitation of ubiquitinated T19N RhoB with introduced lysine mutations. The experiment was performed as in C with the indicated mutants of RhoB. Cells transfected with mCherry and HA-ubiquitin K63 only were used as negative control. **(F)** Quantification of the cell size of HUVECs microporated with mCherry, mCherry-wtRhoB, or mCherry-K162/181R RhoB. Transfected cells were imaged live with an Etaluma 720 lumascope microscope using a 10× dry objective, and cell size was measured cells using ImageJ software (n = 100). **(G)** HUVECs were microporated with the same constructs as in F. Quantification of endothelial resistance measured at 4,000 Hz and normalized to mCherry-transfected cells is shown. Values were obtained in two independent experiments (n = 5 per experiment). **(H)** Immunoblot analysis of the expression of microporated RhoB in HUVECs prepared as in F and treated with NH4Cl for 6 h. Vinculin was used as a loading control. **(I)** Densitometric analysis of RhoB immunoblots from H. Quantification was done using ImageJ software (n = 3). Error bars represent SD. n.s., P ≥ 0.05; ***, P = 0.001–0.0001; ****, P < 0.0001.
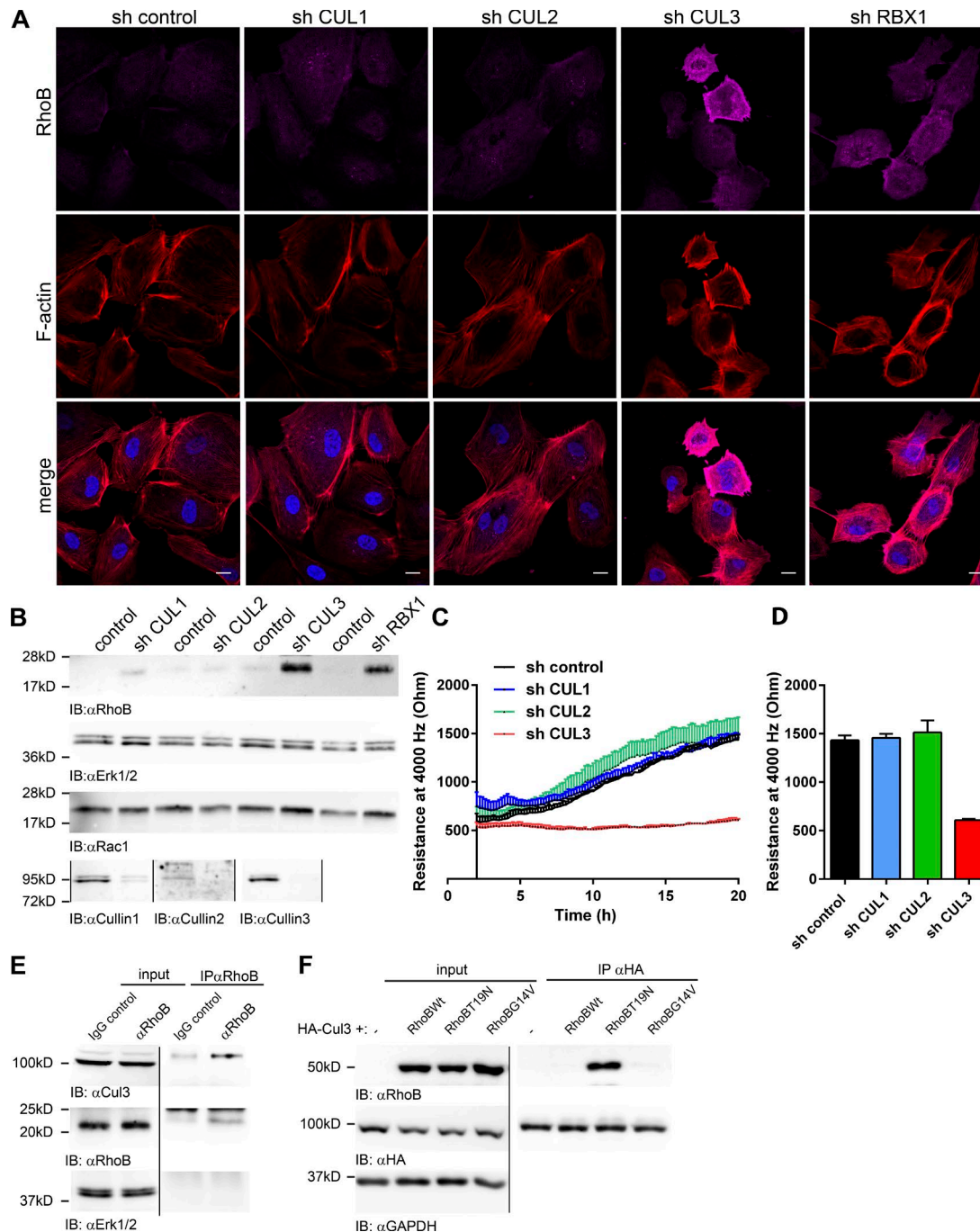
Figure 6. **Cullin-3 is required for degradation of RhoB in ECs. (A)** HUVECs were transduced with control, Cullin-1, Cullin-2, Cullin-3, or RBX1 shRNA, and cells were fixed and stained at 72 h for RhoB (magenta) and F-actin (red). Bars, 15 µm. **(B)** Cells were treated as in A, and lysates were analyzed for RhoB, Cullin1, Cullin-2, Cullin-3, and Rac1. **(C)** HUVECs were treated as in A and seeded in ECIS eight-well arrays at 72 h after infection, and resistance was measured at 4,000 Hz. (*n* = 3). **(D)** Quantification of the measured resistance from C at 20 h after seeding is shown. **(E)** RhoB was immunoprecipitated from lysates of HUVECs, and rabbit IgG antibody was used as a negative control. Input equals 2.5% of the lysate. Samples were analyzed for Cullin-3 and RhoB. **(F)** HEK293T cells were cotransfected with HA-tagged Cullin-3 and mCherry (control) or mCherry-wtRhoB, -T19N RhoB, or -G14V RhoB. 24 h after transfection, HA–Cullin-3 was immunoprecipitated using anti-HA agarose. Input equals 5% of the lysate. Samples were analyzed for RhoB and HA and GAPDH was used as loading control. Error bars represent SD.

positive control, we used Rbx1, a CRL adaptor protein, previously linked to degradation of RhoB in liver cancer cells (Xu et al., 2015). We found that only knockdown of Rbx1 and of Cullin-3, but not Cullin-1 or Cullin-2, significantly increased RhoB expression (Fig. 6, A and B). Moreover, in Cullin-3 knockdown cells, RhoB is not in endosomes (Fig. 6 A) but rather at the plasma membrane, as in cells treated with MLN4924 (Fig. 4,

A–C). In addition, Cullin-3 and Rbx1, but not Cullin-1 or Cullin-2, knockdown ECs displayed increased F-actin stress fiber formation and contractility (Fig. 6 A).

Subsequently, we found that only knockdown of Cullin-3, but not Cullin-1 or Cullin-2, impaired basal monolayer resistance (Fig. 6, C and D). Finally, in coimmunoprecipitation experiments, we detected Cullin-3 in complex with endogenous

RhoB (Fig. 6 E). To confirm these results, we cotransfected HEK293T cells with mCherry-wtRhoB, dominant-negative mCherry-T19NRhoB (Neel et al., 2007), and constitutively active mCherry-G14VRhoB (Neel et al., 2007), together with Cullin-3. We only found the dominant-negative T19N mutant of RhoB in complex with Cullin-3 (Fig. 6 F), in line with the published interaction of inactive RhoA with Cullin-3 in epithelial cells (Chen et al., 2009).

KCTD10 is the substrate receptor for RhoB degradation via Cullin-3 complex in ECs

The role of members of the Bacurd family of proteins KCTD13 and TNFAIP1 in the degradation of RhoA was noted previously (Chen et al., 2009). Therefore, we tested whether knockdown of KCTD13, TNFAIP1, and KCTD10 would influence contractility and RhoB expression in ECs. Loss of KCTD10, but not KCTD13 of TNFAIP1, induced strong actin polymerization and contraction, similar to Cullin-3 knockdown (Fig. 7 A). Cullin-3 and KCTD10 depletion had only a mild effect on RhoA levels, but it induced a sixfold increase in expression of RhoB (Fig. 7, B and C). Knockdown of KCTD13 had no effect, and TNF AIP1 knockdown showed only a slight increase in RhoB expression level (Fig. 7, B and C). Although depletion of Cullin-3 or KCTD10 increased RhoA mRNA levels, it had the opposite effect on RhoB mRNA expression (Fig. S4 B).

Subsequent ECIS analysis showed that KCTD10-depleted ECs displayed a major loss of endothelial barrier function (Figs. 7 D and S4 C). This effect was transient and correlated with the expression levels of RhoB (Fig. 7, B and C). Quantification of endothelial barrier resistance at 72 h after transfection showed that knockdown of KCTD10 induced a 50% loss of resistance when compared with control or knockdown of other Bacurd family members (Figs. 7 E and S4 C). Under these conditions, TNF-α did not reduce barrier function any further (Fig. S5 A). More detailed analysis showed that cell–cell interaction in KCTD10-depleted ECs was strongly decreased (Fig. 7 F). Furthermore, TNFAIP1 knockdown caused a small decrease in Rb parameter values in accordance with the slightly increased RhoB expression in these cells (Fig. 7, B, C, and F).

Furthermore, we tested whether ubiquitination of endogenous RhoB is affected by KCTD10 knockdown. Whereas loss of KCTD10 strongly induced expression of RhoB, its ubiquitination was reduced (Fig. 8 A). To analyze whether RhoB interacts with KCTD10, we transfected HEK293T cells with mCherry-tagged wild-type RhoB, RhoB T19N, or RhoB G14V in combination with HA-tagged Cullin-3 and KCTD10. We detected Cullin-3 and KCTD10 in all samples where RhoB was present (Fig. 8 B). This confirms that RhoB interacts with both Cullin-3 and KCTD10 in vivo. Subsequent rescue experiments showed that overexpression of a siRNA-resistant KCTD10 construct in KCTD10-depleted cells restored RhoB expression to basal levels (Fig. 8 C). In addition, cell contraction and F-actin accumulation induced by KCTD10 depletion were reverted by the siRNA-resistant KCTD10 construct (Fig. 8 D). Moreover, we found that cotransfection of the RhoB targeting siRNA in combination with Cullin-3 or KCTD10 siRNA completely abolished the barrier disruptive effects induced by loss of Cullin-3 or KCTD10 (Fig. 8 E). Finally, we conclude that a Cullin-3–KCTD10 complex mediates degradation of RhoB and is required for the maintenance of endothelial barrier function.

Discussion

Previously, the RhoGTPase RhoA was identified as a key negative regulator of endothelial barrier function via its stimulation of actomyosin contractility through ROCK1/2 activation and subsequent MLC phosphorylation (van Nieuw Amerongen et al., 2000; Birukova et al., 2004). In contrast to RhoA, the function and regulation of RhoB in EC has not been studied extensively. Recently, it was shown that hypoxia induces RhoA and RhoB expression and activity in human microvascular lung ECs (Wojciak-Stothard et al., 2012). RhoB is a short-lived protein with a half-life of 1–2 h (Lebowitz et al., 1995; Engel et al., 1998), in marked contrast to the 24-h half-life of RhoA. Stability of RhoA in HeLa cells is regulated by CRL-mediated ubiquitination and proteasomal degradation of inactive RhoA (Chen et al., 2009). In comparison, hypoxia, TNF-α, or TGF-β stimulation, application of genotoxic agents or inhibitors of isoprenylation all increase the expression of RhoB (Prendergast, 2001; Kroon et al., 2013; Marcos-Ramiro et al., 2016).

Based on these published data, we set out to identify the molecular components of the RhoB degradation machinery in ECs and to define their role in endothelial barrier maintenance (Fig. 9 [working model]). We found that depletion of Cullin-3 significantly reduced basal endothelial resistance and impaired both thrombin- and S1P signaling toward loss or gain, respectively, of endothelial integrity. Cells lacking Cullin-3 showed increased actin stress fiber formation accompanied by increased MLC phosphorylation. Phosphorylated MLC induces actomyosin contractility and formation of actin stress fibers that are structurally and functionally connected to FA complexes (Amado-Azevedo et al., 2014). Our data suggest that Cullin-3 depletion enhances cell contractility and signaling pathways related to FA formation and turnover. In accordance with this, knockdown of Cullin-3 or inhibition of CRLs by MLN4924 induces actin stress fiber formation and increased FA numbers, most probably via increased FA assembly. Simultaneously, AJs are disrupted and endothelial integrity is gradually impaired. We recently found that long-term treatment of HUVECs with MLN4924 decreased protein expression of VE–cadherin, resulting in increased permeability (Sakaue et al., 2017a). In this study, we show that short term-treatment with the drug increased expression of RhoB, resulting in the same phenotype. Thus, the molecular basis underlying increased endothelial permeability induced by MLN4924 depends on the time of exposure to the drug.

The effect of CRL inhibition on the endothelial barrier was dependent on Rho signaling via ROCK1/2. We show that RhoB plays a major role in this pathway, in conjunction with RhoA. Recently, Cullin-2 was identified as a key regulator of RhoB degradation (Xu et al., 2015). In accordance with this, we confirmed the role of another CRL component, Rbx1, but not of Cullin-2, in RhoB degradation in primary HUVECs. Cullin-3 appears the most important regulator of RhoB turnover and signaling output in ECs. These findings indicate that Cullins have specific functions, dependent on tissue-specific expression of Cullin isoforms and substrate receptors.

Cullin-3 interacted most efficiently with inactive RhoB, similar to what was previously described for RhoA (Chen et al., 2009). CUL3-based ubiquitin E3 ligases ubiquitinate their substrates through the formation of a complex with BTB domain–containing proteins (Pintard et al., 2004). Chen et al. (2009) identified BACURD proteins (KCTD13 and TNFAIP1) as substrate receptors for RhoA degradation. However, KCTD13 and
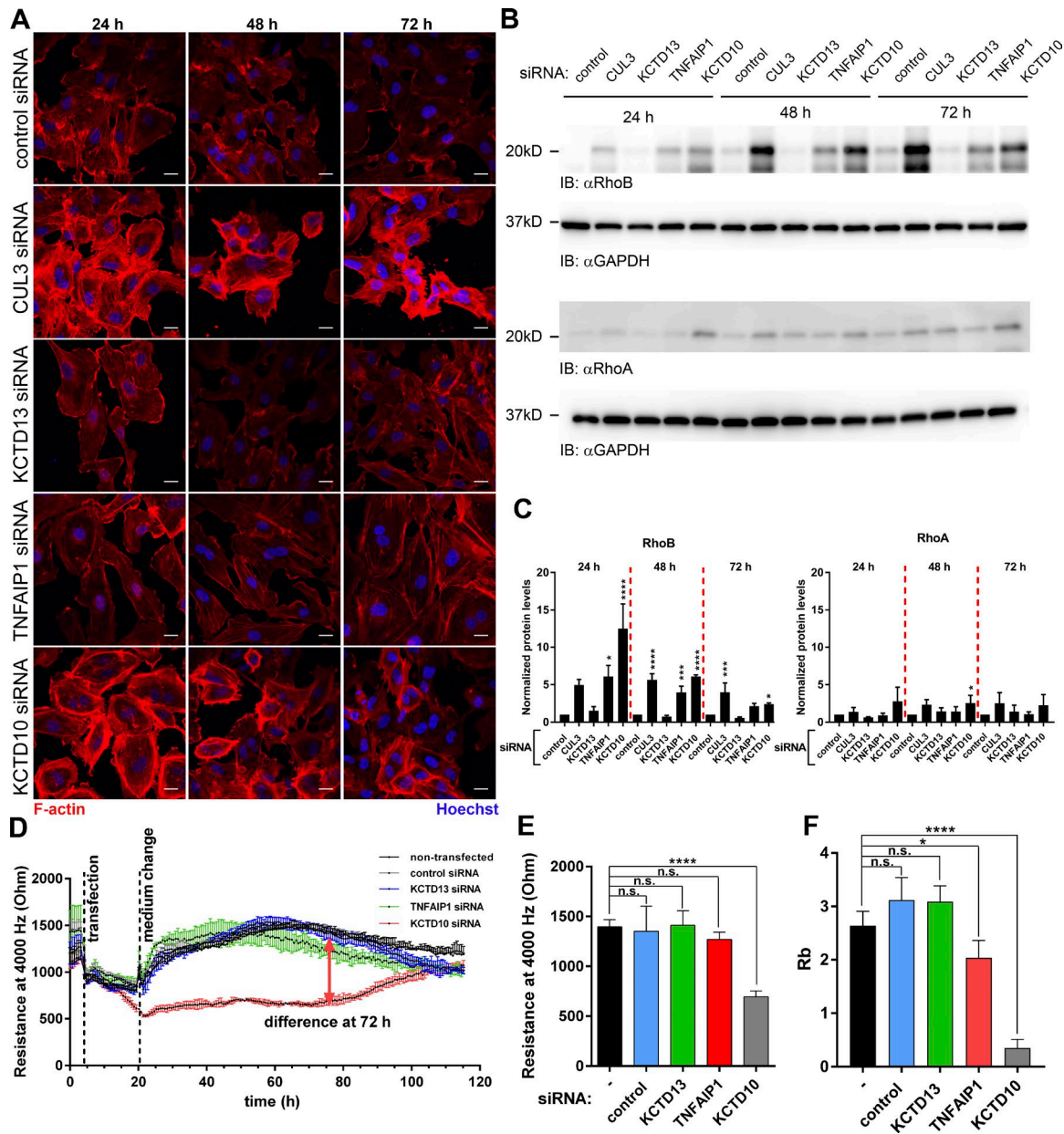
Figure 7. **KCTD10 is a substrate receptor for RhoB in a Cullin-3 complex in ECs. (A)** HUVECs transfected with CUL-3, KCTD13, TNFAIP1, and KCTD10 siRNA were stained for F-actin and nuclei and imaged at 24, 48, and 72 h after transfection. Bars, 20 µm. **(B)** HUVECs were transfected as in A. 15 µg protein was loaded and the membrane was probed for RhoA, RhoB, and GAPDH as loading control. **(C)** Quantification of the RhoA and RhoB immunoblots from B. $n = 3$. **(D)** ECIS measurement (4,000 Hz) of HUVECs transfected with siRNAs as in A. **(E)** Quantification of resistance at 72 h after transfection of HUVECs prepared as in A. **(F)** Analysis of the Rb parameter was performed as in F. Error bars represent SD. n.s., $P \geq 0.05$; *, $P = 0.01–0.05$; ***, $P = 0.001–0.0001$; ****, $P < 0.0001$.

TNFAIP1 did not mediate degradation of RhoB in ECs. We found KCTD10 to be most relevant as substrate receptor for the ubiquitination and degradation of RhoB. KCTD10 contains a BTB/POZ domain and regulates cardiovascular development in zebrafish and mouse (Hu et al., 2014; Ren et al., 2014; Tong et al., 2014). Although different substrates were proposed to mediate the effects of loss of KCTD10 in these animal models, RhoGTPases were suggested as potential targets of KCTD10 in regulation of cardiovascular development. Our current findings corroborate this suggestion by underscoring the role of KCTD10 in regulating RhoB.

Deletion of RhoB in mice did not have detrimental effects on development and fertility, possibly because of a compensatory role of other RhoGTPase family members (Liu et al., 2000; Pronk et al., 2017). However, these mice do display defects in vascular sprouting in the retina, impaired morphology of neurons, and thymus atrophy (Adini et al., 2003; McNair et al., 2010; Bravo-Nuevo et al., 2011). In contrast to these relatively mild effects, recent publications show that increased expression of RhoB correlates with human pathologies and can even cause fatal disease, such as capillary leak syndrome (Yang et al., 2013a; Marcos-Ramiro et al., 2016; Mandik-Nayak et al., 2017; Pierce et al., 2017).

RhoB expression is increased not only by CRL-mediated inhibition of RhoB degradation but also by TNF-α–induced transcription and translation (Fig. S5 B). The subcellular local-
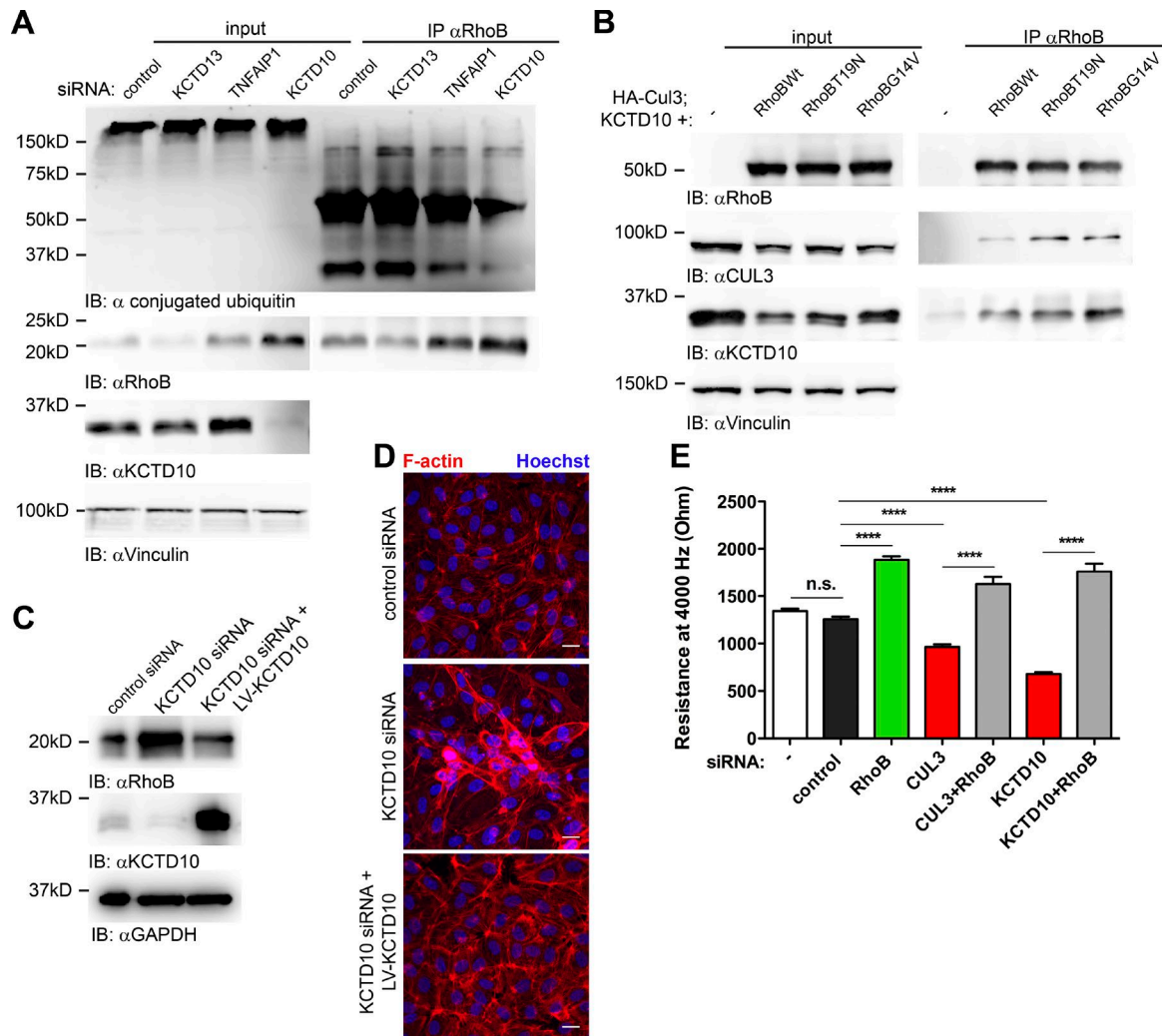
Figure 8. Degradation of RhoB via Cullin-3–KCTD10 complex is required for maintenance of endothelial barrier function. (A) Cells were transfected with KCTD13, TNFAIP1, KCTD10, or control siRNA. 72 h after transfection, cells were treated with 5 µM MG132 for 4 h, followed by 2.5 µM PR619 for 2 h. RhoB was immunoprecipitated, and samples were analyzed for ubiquitination with ubiquitin FK-2 antibody. **(B)** HEK293T cells were cotransfected with HA-tagged Cullin-3, KCTD10, and mCherry-wtRhoB, mCherry-RhoB-T19N, and mCherry-RhoB-G14V. 24 h after transfection, RhoB was immunoprecipitated using polyclonal RhoB antibody. Input equals 5% of the lysate used for immunoprecipitation. Samples were analyzed using RhoB, Cullin-3, and KCTD10 antibodies. **(C)** Immunoblot (IB) analysis of the RhoB expression in the KCTD10-rescue experiment. KCTD10 constructs corresponding to LV-KCTD10 or empty vector were expressed in HUVECs using the Lentivirus gene expression system. Control siRNA or siRNA targeting the 3′ UTR of KCTD10 was transfected into the cells. GAPDH immunoblot is shown as loading control. **(D)** Cells were prepared as in C. After 72 h, cells were fixed and stained for F-actin (red) and nuclei (blue). Bars, 20 µm. **(E)** HUVECs were transfected with single siRNA or combinations of siRNAs as shown in the graph, and endothelial monolayer resistance was measured using ECIS at 72 h after transfection. Error bars represent SD. n.s., P ≥ 0.05; ****, P < 0.0001.

ization of RhoB under these conditions is different. Although in unstimulated cells, RhoB is in lysosomes, as it is in TNF-α–stimulated cells, inhibition of CRL-mediated RhoB degradation in resting cells induced its translocation to the cytoplasm and the plasma membrane. In our experiments, lysosomal localization of RhoB was almost completely abolished by the inhibition of CRLs, suggesting that the CRL-dependent ubiquitination of RhoB controls, in addition to proteasomal degradation, its lysosomal targeting and degradation. Furthermore, we could show that TNF-α induces colocalization of RhoB with K63-polyubiquitination–positive endosomes, which was lost upon CRL inhibition. Importantly, TNF-α does not act by inhibiting CRL-mediated ubiquitination of RhoB. In contrast, TNF-α increases the level of RhoB mRNA and thus RhoB protein. In agreement with this, we found that RhoB is preferentially polyubiquitinated by K63-specific linkage, independent of

TNF-α, which was largely inhibited by MLN4924. K63-linked polyubiquitination was described to target proteins toward the lysosomal degradation pathway via their interaction with the ESCRT machinery (Nathan et al., 2013). Although the CRLs are traditionally referred to as K48-linkage–specific E3 ligases, different type of linkages mediated by this set of enzymes were described previously (Jin et al., 2009; Yuan et al., 2014). To our knowledge, our study is the first one to describe CRL-dependent K63 polyubiquitination of RhoGTPases in ECs.

Differential localization (endosomal vs. plasma membrane) of RhoB and differential functionality depending on its cellular locale was postulated previously (Lebowitz et al., 1997; Du and Prendergast, 1999; Wherlock et al., 2004). We found that the increased expression and membrane association of RhoB caused by inhibition of CRLs indeed leads to a significant increase in its activity. These findings suggest that in resting
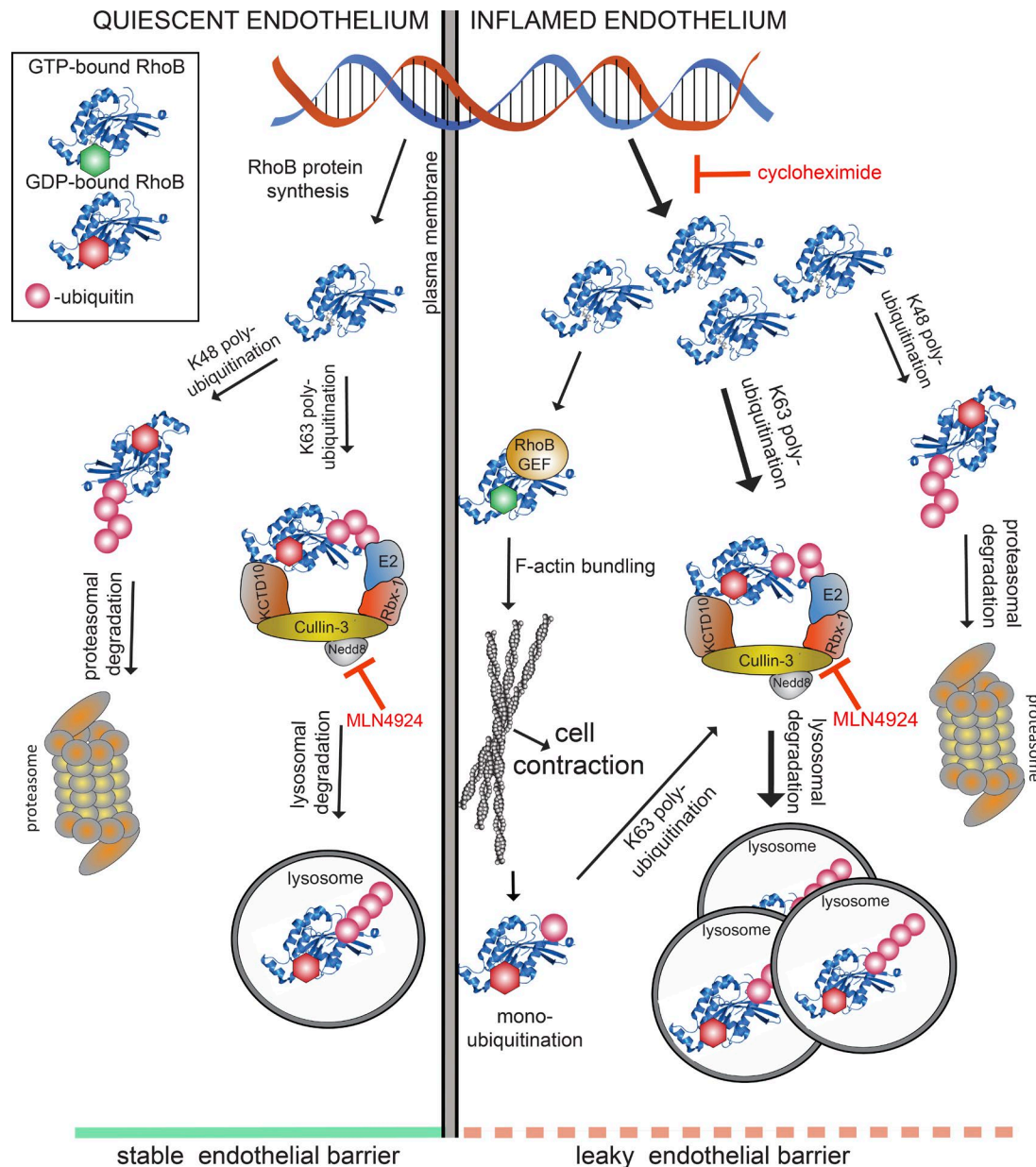
Figure 9.   **Model for CUL3/KCTD10-mediated ubiquitination of RhoB and its subsequent lysosomal degradation in maintenance of endothelial barrier function.** RhoB is expressed at very low levels in quiescent endothelium (left side of the model) and is efficiently degraded via the proteasome and lysosomes because of CUL3/KCTD10-dependent K63 ubiquitination. As a result, the endothelial barrier remains intact. Inflammatory cytokines (e.g., TNF-α) enhance the expression of RhoB in ECs (right side of the model), and a fraction of RhoB escapes ubiquitination by CUL3/KCTD10 and subsequent lysosomal degradation. This remaining, active RhoB is associated with the plasma membrane and promotes formation of F-actin stress fibers, which results in disruption of endothelial barrier. Ribbon structure of RhoB (aa 4–187) was obtained from the Protein Data Bank (2FV8). GEF, guanine nucleotide exchange factor.

ECs, RhoB is expressed at low levels and is localized, in nonubiquitinated form, outside of lysosomes, in part at the plasma membrane, where it exerts its activity (Fig. 9). Low levels of RhoB are maintained via constant CRL-dependent ubiquitination, subsequent targeting to lysosomes and degradation. This is supported by the increased formation of stress fibers upon CRL inhibition. CRL inhibition leads to RhoB up-regulation and activation, inducing contraction and impaired endothelial barrier stability. In contrast, TNF-α induces de novo synthesis of RhoB accompanied by limited RhoB activation (Figs. 9 and S5 B). In line with this, the negative effects of TNF-α on endothelial barrier function are also more limited than those induced by inhibition of CRL-mediated RhoB degradation.

The C terminus of RhoB encodes the signal that determines its localization and degradation (Lebowitz et al., 1995; Michaelson et al., 2001). This fact and the apparent role of ubiquitination in the regulation of RhoB localization and degradation led us to hypothesize that the lysine acceptor site for RhoB ubiquitination is located at the C terminus. Furthermore, the increased turnover of RhoB could be caused by additional ubiquitin acceptor sites specific for RhoB. Because Lys181 is only present in RhoB and not in RhoA or RhoC, we decided to mutate Lys181 and other lysines in the C-terminal half of RhoB, the side chains of which are exposed at the surface of the molecule (Lys135 and Lys162). We found that mutation of only Lys162 or Lys181 significantly impairs the efficiency

of RhoB K63-specific polyubiquitination, suggesting that the short half-life of RhoB protein is caused by efficient ubiquitination of RhoB at multiple lysine acceptor sites followed by lysosomal degradation.

Ubiquitination-dependent regulation of RhoGTPases was previously studied only in the context of proteasomal degradation (Wang et al., 2006; Chen et al., 2009; Oberoi et al., 2012). We and others showed that ubiquitination might target Rac1 to an endosomal compartment (Nethe and Hordijk, 2010; Baker et al., 2013). To our knowledge this study is the first to report the K63-linkage–specific polyubiquitination and subsequent lysosomal degradation of a RhoGTPase. Novel, specific inhibitors targeting components of the ubiquitination machinery may provide new options for treatment of various human pathologies. A crucial goal in these efforts should be to identify determinants of specificity, especially in terms of substrate-binding receptors in ubiquitin ligase complexes such as CRLs. Here, we show that the specificity of the substrate recognition can be very strict, even among a highly conserved group of proteins such as the RhoA, RhoB, and RhoC GTPases.

Materials and methods

Cell culture
HUVECs were purchased from Lonza and cultured on fibronectin-coated dishes at 37°C in 5% CO_2 atmosphere. EGM2 medium supplemented with SingleQuots (Lonza) was used for culturing HUVECs. Cells were used for experiments until passage 5. HEK293T cells were purchased from ATCC and cultured in Iscove's modified Dulbecco's medium (Lonza) supplemented with 10% FCS and L-glutamine. Cells were used until passage 35 for production of lentiviral particles, native coimmunoprecipitation and immunoprecipitation of ubiquitinated proteins under denaturing conditions.

Antibodies
The following primary antibodies were used in this study: mouse αVE–cadherin/CD144–Alexa Fluor 647 (BD), rabbit αErk1/2 (Santa Cruz), mouse αpErk1/2 (Santa Cruz), rabbit αpMyosin LC2 Thr18/Ser19 (Cell Signaling), rabbit αpPAK1/2/3 Ser141 (Invitrogen), rabbit αvinculin (Sigma), rabbit αGAPDH (Cell Signaling), mouse αHA (Sigma), rabbit αLAMP1 (Cell Signaling), rabbit αKCTD10 (Sigma), rabbit αPaxillin Tyr31 (Sigma), mouse αRac1 (BD), rabbit αRhoC (Cell Signaling), rabbit αRhoA (Cell Signaling), rabbit αRhoB (Santa Cruz), mouse αRhoB (Santa Cruz), mouse αUbiquitin (FK-2; Boston Biochem), rabbit αUbiquitin, Lys63-specific (Apu3; Millipore), rabbit αCullin-3 (Cell Signaling), mouse αCullin-2 (BD), mouse αCullin-1 (Santa Cruz), rabbit αKCTD10 (Sigma), rat αmouseCD29 (9eg7; BD), rabbit αIntegrin α-5 (Abcam), and rabbit p-NF-κB p65 (Ser536; Cell Signaling). Mouse anti–HA agarose was purchased from Sigma.

Lentiviral shRNA constructs
Lentiviral shRNA constructs were obtained from the TRC/Sigma Mission library (Sigma). All the constructs were cloned into pLKO.1 vector. The following clones were used in this study: BIRC2 TRCN00003780 and TRCN0000320867, XIAP TRCN00003785 and TRCN0000231578, FBXW7 TRCN0000355641, TRCN0000355643 and TRCN0000355644, CUL1 TRCN0000318414 and TRCN0000318416, Cullin-3 TRCN-0000288625 and TRCN0000307983, BTRC TRCN00006543 and TRCN00006545, USP8 TRCN0000284767 and TRCN0000284769, CYLD TRCN0000230278, TRCN0000230279, TRCN0000230280 and TRCN0000230281, TRIP12 TRCN0000273210 and TRCN0000273135,

TNFAIP3 TRCN000050961, OTULIN TRCN0000275410 and TRCN0000275411, FBXL19 TRCN000062336 and TRCN0000359134, SMURF2 TRCN00003478 and TRCN0000272880, HACE1 TRCN-00003415, TRCN0000415313 and TRCN0000427070, RABGEF1 TRCN000047237, TRCN0000419718 and TRCN0000422664, SMURF1 TRCN00003471 and TRCN00003473, USP17L2 TRCN0000376547, CBL TRCN0000288695, KIA0317 TRCN0000280035, NEDD4L TRCN0000904, NEDD4 TRCN0000905 and TRCN00007550, and CAV1 TRCN00008002 and TRCN000011218. As a negative control, nontargeting shRNA TRCN0000SHC002 was used.

Lentivirus production
Lentiviral particles were produced by transfecting HEK293T cells with the third-generation HIV-1 packaging plasmids (Addgene) using Trans IT (Mirus). Cell culture medium containing virus particles was collected at 48 and 72 h after transfection, centrifuged, and filtered through 0.45-µm polyvinylidene fluoride filter (Millipore). Supernatant containing lentivirus was used to infect subconfluent HUVECs. Infected HUVECs were used for experiments at 72 h after infection. All shRNA clones that were used in the study were verified by sequencing (45 clones targeting 22 proteins) and are shown in Fig. S1 B . The identity of 7 clones used in the screen could not be validated by sequencing and is therefore omitted from Fig. S1 B and the phenotype analysis. The efficiency of the knockdown in several cases was assessed by immunoblotting.

For KCTD10 lentiviral overexpression, KCTD10 cDNA was cloned into a CSII-CMV-MCS-IRES2-Bsd vector and packed into lentivirus particles as described previously (Sakaue et al., 2017b). Lentiviral expression and packaging vectors were kindly provided by H. Miyoshi (RIKEN BioResource Center, Wako, Japan). Template cDNA (product ID FHC07641) was purchased from Kazusa DNA Research Institute.

Immunoblotting
Cell lysates for immunoblotting were collected by lysing cells in sample buffer (125 mM Tris, pH 6.8, 20% glycerol, 4% βmercapto-EtOH, and 0.001% bromophenol blue). Lysates were separated using SDS-PAGE on 7% or 12% polyacrylamide gels and transferred to the nitrocellulose membrane. Membranes were blocked in 5% BSA in TBST-T for 1 h and probed with primary antibodies diluted in the blocking buffer overnight at 4°C. Proteins were visualized using secondary anti–rabbit or anti–mouse antibodies coupled to the HRP and x-ray films. Densitometric analysis of the band intensities was performed using ImageJ.

Endothelial barrier integrity measurement
Measurement of the integrity of endothelial barrier was performed using ECIS. For this assay, 100,000 HUVECs were seeded in fibronectin-coated eight-well ECIS slides (Applied Biophysics). Slides were mounted into the ECIS Zθ (theta) instrument, and the resistance of the electrodes was monitored at multiple frequencies at 37°C during next 48 h. At 16–18 h, upon seeding, cells formed a stable monolayer, and resistance at 4,000 Hz was used to compare the barrier integrity among different samples. For thrombin stimulation, cells were treated with 1 U/ml thrombin (Sigma). S1P response was assessed by adding 500 nM S1P to the cells. As the last parameter, wounding recovery was measured. In this assay, the HUVEC monolayer was wounded electrically at 100,000 Hz and 6,500 µA for 2 min, and the recovery of the wounded area was monitored over the next 6 h. The Rb values were obtained by modeling from the multiple frequency scans using ECIS software from Applied Biophysics.

siRNA transfection and chemical inhibition of Rho signaling
For these experiments, HUVECs were freshly isolated from umbilical cords as previously described (Draijer et al., 1995) and used

for experiments at passage 2. siRNA SMART pools targeting RhoA (L-008555-00-0005), RhoB (L-008395-00-0005), and RhoC (L-003860-00-0005) and ON-TARGETplus Non-targeting Pool control siRNA (D-001810-10-05) were purchased from Dharmacon. siR-NAs targeting CUL3, KCTD13 (SASI_Hs01_00120957), TNFAIP1 (SASI_Hs01_00131786), KCTD10 (custom-made, sense sequence: 5′-GUAACAACAAAUACUCAUATT-3′), siRNA sequence targeting the 3′ UTR of KCTD10 (sense sequence: 5′-GAAUGAGCG UCUAAAUCGUTT-3′), and control siRNA (SIC-001) were all purchased from Sigma. Additional siRNAs targeting KCTD10 (siRNA 1, HSS130450; siRNA 2, IHSS130452; and siRNA 3, HSS188856) and control siRNA L (12935-200) and siRNA M (12935-300) were all purchased from Invitrogen.

HUVECs were seeded on gelatin-coated eight-well ECIS slides (Applied Biophysics) at 60–70% confluency and transfected with final concentration of 25 nM siRNA using DharmaFECT (Dharmacon). ECIS measurement and MLN4924 treatment was performed 72 h after transfection. Because of the high concentration of serum (20%) in the medium, cells were starved in serum-free medium containing 1% human serum albumin for 24 h before the addition of 500 nM MLN4924.

For chemical inhibition of ROCK1/2 or RhoGTPases with 10 µM Y-27632 or 1 µg/ml C3-transferase, respectively, HUVECs were seeded on gelatin-coated eight-well ECIS slides (Applied Biophysics) and grown to confluency. Before the addition of inhibitors, cells were starved for 1.5 h and then treated with Y-27632 or C3-transferase for 30 min, followed by addition of 500 nM MLN4924.

Immunofluorescence
For immunofluorescence analysis, HUVECs were seeded on fibronectin-coated 12-mm glass coverslips. Cells were treated with 300 nM MLN4924, 10 ng/ml TNF, or combination of both for 4 or 18 h For activated β1-integrin staining, cells were stimulated with 500 nM S1P for 15 min. Cells were briefly washed in PBS containing 1 mM $CaCl_2$ and 0.5 mM $MgCl_2$ and fixed for 15 min with 4% PFA. Upon fixation, cells were permeabilized with 0.2% Triton X-100 in PBS for 3 min and unspecific staining was blocked by incubation with 1% BSA in PBS for 30 min. Primary antibody incubation was done in blocking buffer for 1 h, followed by extensive washing and incubation with secondary antibody for 30 min. Secondary antibodies used in this study were goat anti–mouse Alexa Fluor 488, goat anti–rabbit Alexa Fluor 568, and goat anti–rabbit Alexa Fluor 488 (all from Invitrogen). Hoechst was used to stain nuclei and phalloidin Alexa Fluor 415 (Promokine) or phalloidin Texas red (Invitrogen) to stain F-actin. Lysotracker Red DND-99 (Molecular Probes) was used to mark acidic/late endosomes. After washing in 0.1% BSA in PBS, coverslips were mounted in MOWIOL supplemented with DABCO and analyzed by confocal microscope Leica SP8 using 63×/1.4 or 100×/1.4 oil-immersion objective or Nikon A1R using 63 × 1.4 oil-immersion objective. Image analysis was done in ImageJ.

Live fluorescence microscopy of FA dynamics
HUVECs were infected with nontargeting control or CUL-3 shRNA. Cells were seeded on fibronectin coated eight-well Lab Tek chambers (Thermo Fisher Scientific) and at 72 h after infection transfected with pEGFP-C3 vinculin construct (E. Danen, University of Leiden, Leiden, Netherlands) using TransIT (Mirus). The next day, cells were imaged for 20 min at intervals of 20 s using an Observer Z1 microscope (Zeiss) equipped with 40× oil-immersion objective. Still images were uploaded on the FA analysis server (http://faas.bme.unc.edu/), and analysis of FA turnover was performed as previously described (Berginski et al., 2011; Berginski and Gomez, 2013). In brief, FAs were identified based on EGFP-vinculin positivity within thresholded images of single cells. To distinguish single cells, masks were created from the overexposed signal

of EGFP-vinculin. Dynamic properties (assembly and disassembly rate) of FAs were obtained by the tracking of changes in intensity of the fluorescence from single adhesions through subsequent image frames. Four cells per condition were imaged and analyzed.

Microporation of ECs
Microporation of HUVECs was performed using Amaxa 4D nucleofector and P5 Primary-Cell Nucleofector X-kit (Lonza). A 20-cm^2 area of subconfluent HUVECs was trypsinized and microporated with 1.5 µg mCherry, mCherry-wtRhoB or mCherry-K162/181R RhoB. The cells were immediately seeded either on fibronectin-coated ECIS slides for measurement of the barrier resistance or on 24-well plate containing fibronectin-coated glass slides for immunofluorescence imaging.

Real-time PCR analysis
HUVECs were treated with DMSO or MLN4924 (0.3 and 0.6 µM), control siRNA, CUL3 siRNA, and KCTD10 siRNA for 72 h. Total RNAs were purified from the HUVECs using ISOGEN II (Nippon Gene) as described previously (Sakaue et al., 2017b). In brief, 1 µg RNA was used for first-strand cDNA synthesis using the High Capacity RNA-to-cDNA Master Mix (Applied Biosystems). Real-time quantitative PCR was performed (FastStart Universal SYBR Green Master ROX; Roche Diagnostics) with the ABI 7300/7500 system (Applied Biosystems). The following primers were used for amplification: 5′-GAGGTGGATGGAAAGCAGGTAGAGTTG-3′ (RhoA-F), 5′-TTT CACCGGCTCCTGCTTCATCTTGG-3′ for (RhoA-R) for RhoA and 5′-AGACGTGCCTGCTGATCGTGTTCAG-3′ (RhoB-F) and 5′-CAC ATTGGGACAGAAGTGCTTCACC-3′ (RhoB-R) for RhoB, and 5′-TGCACCACCAACTGCTTAGC-3′ (GAPDH-F) and 5′-GGCATG GACTGTGGTCATGAG-3′ (GAPDH-R) for GAPDH.

Immunoprecipitation
Immunoprecipitation of endogenous RhoB was performed with rabbit αRhoB antibody (Santa Cruz) from confluent 60-cm^2 dishes. Before lysis, cells were stimulated with either 10 ng/ml TNF-α (Peprotech) or 300 nm MLN4924 for 4 h or 2.5 µM PR619 for 2 h. Proteasomal degradation was inhibited by adding 5 µM MG132 at 2 h before lysis. Upon stimulation, cells were washed in PBS containing 1 mM $CaCl_2$ and 0.5 mM $MgCl_2$ and lysed in lysis buffer (50 mM Tris, pH 7.4, 150 mM NaCl, 1 mM EDTA, and 1% NP-40), cOmplete Protease Inhibitor Cocktail Tablets (Roche), and phosphatase inhibitors (1 mM Na_3VO_4 and 25 mM NaF). Lysates were cleared by centrifugation and incubated with 1 µg RhoB antibody for 2 h at 4°C. RhoB containing complexes were pulled out by incubation with Dynabeads protein G (Thermo Fisher Scientific) for 1 h at 4°C. Finally, beads were washed four times with lysis buffer, and immunoprecipitated proteins were eluted with sample buffer and analyzed with SDS-PAGE.

Mutagenesis
Single mutants of RhoB K135R, K162R, and K181R were generated using the site-directed mutagenesis. Mutations were introduced into the pmCherryC1-T19N RhoB vector in a PCR reaction using site-specific primers (Invitrogen) and high-fidelity Phusion DNA polymerase (NEB). Template DNA was digested by DpnI (NEB), and PCR product was transformed into competent DH5α *Escherichia coli* (NEB). Bacterial colonies were screened for presence of the desired mutation by DNA sequencing.

HA-tag native immunoprecipitation
For HA-tag immunoprecipitation, pmCherryC1-RhoB, pmCherryC1-RhoB-T19N, or pmCherryC1-RhoB-G14V (gift of N. Reinhard, Swammerdam Institute for Life Sciences, Amsterdam, Netherlands)

was cotransfected with NTAP-HA-CUL3 (gift of H. Genau, Goethe University Medical School, Frankfurt am Main, Germany). For native coimmunoprecipitation, transfected cells were lysed in lysis buffer (150 mM NaCl, 50 mM Tris, pH 7.4, 1 mM EDTA, 5% glycerol, and 1% IGEPAL) supplemented with protease inhibitor complex (Roche). Lysates were cleared by centrifugation and incubated with mouse anti-HA agarose beads (Sigma) for 3 h at 4°C. Upon incubation, beads were washed four times with the lysis buffer and boiled in 50 µl sample buffer, and samples were analyzed by immunoblotting.

In vivo ubiquitination assay

For this assay pcDNA3-HA-K48only-ubiquitin or pcDNA3-HA-K63only ubiquitin (gift of K. Husnjak, Goethe University Medical School, Frankfurt am Main, Germany) were cotransfected with pmCherryC-1, pmCherryC1-RhoB-T19N, pmCherryC1-RhoB-T19N;K135R, pmCherryC1-RhoB-T19N;K162R, or pmCherryC1-RhoB-T19N;K181R into HEK293T cells using TransIT (Mirus) according to the manufacturer's protocol. Before lysis, cells were treated with 10 µM MG132 in combination with or without 500 nM MLN4924 for 6 h For analysis of ubiquitination of RhoB and mutants thereof, denaturing HA-immunoprecipitation was performed at 24 h after transfection as previously described (Genau et al., 2015).

RhoGTPase and Rac activation assays

For the RhoGTPase activation assay, cells were stimulated with 10 ng/ml TNF-α (Peprotech) or 300 nm MLN4924 for 4 h or 2.5 µM PR619 for 2 h and lysed in cold lysis buffer (25 mM Tris-HCl, pH 7.2, 150 mM NaCl, 10 mM MgCl$_2$, 1% NP-40, and 5% glycerol) supplemented with cOmplete Protease Inhibitor Cocktail Tablets (Roche).

To analyze Rac activity, HUVECs were treated the same as for the RhoGTPase activation assay and levels of Rac1-GTP were measured by PAK1-CRIB pull-down assay as previously described (de Kreuk et al., 2013).

Statistical analysis

All graphs in the figures represent means ± SD. Statistical analysis was performed using GraphPad Prism software. For comparison of only two groups of samples, the two-tailed Student's *t* test was applied. One-way ANOVA with Tukey's post-tests was applied when more than two groups were compared (n.s., P ≥ 0.05; *, P = 0.01–0.05; **, P = 0.01–0.001; ***, P = 0.001–0.0001; ****, P < 0.0001).

Online supplemental material

Fig. S1 shows the workflow of targeted shRNA screen for EC morphology regulators, the table with used constructs, an example of positive hit and additional shRNA clone targeting CUL3. Fig. S2 shows FA staining in CUL3 KD cells, VE–cadherin staining, and RhoA protein stability analysis upon MLN4924 treatment and RhoB immunoblot upon cycloheximide and TNF-α treatment. Fig. S3 shows knockdowns of RhoA, RhoB, and RhoC using siRNA, the effect of combined double (RhoA/B, RhoA/C, and RhoB/C) and triple (RhoA/B/C) knockdowns on MLN4924-induced endothelial barrier loss, the effect of Y27 and C3 on MLN4924-induced loss of endothelial barrier, analysis of Rac1 activity upon MLN4924 treatment, and quantification of immunoblots from Fig. 4 E. Fig. S4 shows RhoB ubiquitination assay with TNF-α stimulation and effects of additional KCTD10 siRNAs on the endothelial barrier. Fig. S5 shows ECIS measurement on KCTD10 knockdown cells treated with TNF-α and a model for TNF-α's role in the regulation of RhoB expression. Videos 1 and 2 show FA dynamics in control and CUL3 knockdown cells, respectively.

References

Adini, I., I. Rabinovitz, J.F. Sun, G.C. Prendergast, and L.E. Benjamin. 2003. RhoB controls Akt trafficking and stage-specific survival of endothelial cells during vascular development. *Genes Dev.* 17:2721–2732. https://doi.org/10.1101/gad.1134603

Amado-Azevedo, J., E.T. Valent, and G.P. Van Nieuw Amerongen. 2014. Regulation of the endothelial barrier function: a filum granum of cellular forces, Rho-GTPase signaling and microenvironment. *Cell Tissue Res.* 355:557–576. https://doi.org/10.1007/s00441-014-1828-6

Baker, R., S.M. Lewis, A.T. Sasaki, E.M. Wilkerson, J.W. Locasale, L.C. Cantley, B. Kuhlman, H.G. Dohlman, and S.L. Campbell. 2013. Site-specific monoubiquitination activates Ras by impeding GTPase-activating protein function. *Nat. Struct. Mol. Biol.* 20:46–52. https://doi.org/10.1038/nsmb.2430

Beckers, C.M., V.W. van Hinsbergh, and G.P. van Nieuw Amerongen. 2010. Driving Rho GTPase activity in endothelial cells regulates barrier integrity. *Thromb. Haemost.* 103:40–55. https://doi.org/10.1160/TH09-06-0403

Berginski, M.E., and S.M. Gomez. 2013. The Focal Adhesion Analysis Server: a web tool for analyzing focal adhesion dynamics. *F1000 Res.* 2:68.

Berginski, M.E., E.A. Vitriol, K.M. Hahn, and S.M. Gomez. 2011. High-resolution quantification of focal adhesion spatiotemporal dynamics in living cells. *PLoS One.* 6:e22025. https://doi.org/10.1371/journal.pone.0022025

Birukova, A.A., K. Smurova, K.G. Birukov, K. Kaibuchi, J.G. Garcia, and A.D. Verin. 2004. Role of Rho GTPases in thrombin-induced lung vascular endothelial cells barrier dysfunction. *Microvasc. Res.* 67:64–77. https://doi.org/10.1016/j.mvr.2003.09.007

Bolte, S., and F.P. Cordelières. 2006. A guided tour into subcellular colocalization analysis in light microscopy. *J. Microsc.* 224:213–232. https://doi.org/10.1111/j.1365-2818.2006.01706.x

Bravo-Nuevo, A., R. O'Donnell, A. Rosendahl, J.H. Chung, L.E. Benjamin, and C. Odaka. 2011. RhoB deficiency in thymic medullary epithelium leads to early thymic atrophy. *Int. Immunol.* 23:593–600. https://doi.org/10.1093/intimm/dxr064

Chen, Y., Z. Yang, M. Meng, Y. Zhao, N. Dong, H. Yan, L. Liu, M. Ding, H.B. Peng, and F. Shao. 2009. Cullin mediates degradation of RhoA through evolutionarily conserved BTB adaptors to control actin cytoskeleton structure and cell movement. *Mol. Cell.* 35:841–855. https://doi.org/10.1016/j.molcel.2009.09.004

Chen, Y.Z., Z.X. Yang, M. Meng, Y. Zhao, N. Dong, H.M. Yan, L.P. Liu, M.X. Ding, H.B. Peng, and F. Shao. 2011. Cullin Mediates Degradation of RhoA through Evolutionarily Conserved BTB Adaptors to Control Actin Cytoskeleton Structure and Cell Movement. *Mol. Cell.* 44:1005–1005. https://doi.org/10.1016/j.molcel.2011.12.001

Cherfils, J., and M. Zeghouf. 2013. Regulation of small GTPases by GEFs, GAPs, and GDIs. *Physiol. Rev.* 93:269–309. https://doi.org/10.1152/physrev.00003.2012

Clark, P.R., R.K. Kim, J.S. Pober, and M.S. Kluger. 2015. Tumor necrosis factor disrupts claudin-5 endothelial tight junction barriers in two distinct NF-κB-dependent phases. *PLoS One.* 10:e0120075. https://doi.org/10.1371/journal.pone.0120075

Coughlin, S.R. 1999. How the protease thrombin talks to cells. *Proc. Natl. Acad. Sci. USA.* 96:11023–11027. https://doi.org/10.1073/pnas.96.20.11023

de Bie, P., and A. Ciechanover. 2011. Ubiquitination of E3 ligases: self-regulation of the ubiquitin system via proteolytic and non-proteolytic mechanisms. *Cell Death Differ.* 18:1393–1402. https://doi.org/10.1038/cdd.2011.16

Dejana, E., G. Bazzoni, and M.G. Lampugnani. 1999. Vascular endothelial (VE)-cadherin: only an intercellular glue? *Exp. Cell Res.* 252:13–19. https://doi.org/10.1006/excr.1999.4601

de Kreuk, B.J., A. Schaefer, E.C. Anthony, S. Tol, M. Fernandez-Borja, D. Geerts, J. Pool, L. Hambach, E. Goulmy, and P.L. Hordijk. 2013. The human minor histocompatibility antigen 1 is a RhoGAP. *PLoS One.* 8:e73962. https://doi.org/10.1371/journal.pone.0073962

Draijer, R., A.B. Vaandrager, C. Nolte, H.R. de Jonge, U. Walter, and V.W. van Hinsbergh. 1995. Expression of cGMP-dependent protein kinase I and phosphorylation of its substrate, vasodilator-stimulated phosphoprotein, in human endothelial cells of different origin. *Circ. Res.* 77:897–905. https://doi.org/10.1161/01.RES.77.5.897

Du, W., and G.C. Prendergast. 1999. Geranylgeranylated RhoB mediates suppression of human tumor cell growth by farnesyltransferase inhibitors. *Cancer Res.* 59:5492–5496.

Engel, M.E., P.K. Datta, and H.L. Moses. 1998. RhoB is stabilized by transforming growth factor beta and antagonizes transcriptional activation. *J. Biol. Chem.* 273:9921–9926. https://doi.org/10.1074/jbc.273.16.9921

Essler, M., J.M. Staddon, P.C. Weber, and M. Aepfelbacher. 2000. Cyclic AMP blocks bacterial lipopolysaccharide-induced myosin light chain phosphorylation in endothelial cells through inhibition of Rho/Rho kinase signaling. *J. Immunol.* 164:6543–6549. https://doi.org/10.4049/jimmunol.164.12.6543

Genau, H.M., J. Huber, F. Baschieri, M. Akutsu, V. Dötsch, H. Farhan, V. Rogov, and C. Behrends. 2015. CUL3-KBTBD6/KBTBD7 ubiquitin ligase cooperates with GABARAP proteins to spatially restrict TIAM1-RAC1 signaling. *Mol. Cell.* 57:995–1010. https://doi.org/10.1016/j.molcel.2014.12.040

Hirano, S., N. Kimoto, Y. Shimoyama, S. Hirohashi, and M. Takeichi. 1992. Identification of a neural alpha-catenin as a key regulator of cadherin function and multicellular organization. *Cell.* 70:293–301. https://doi.org/10.1016/0092-8674(92)90103-J

Hordijk, P.L., E. Anthony, F.P. Mul, R. Rientsma, L.C. Oomen, and D. Roos. 1999. Vascular-endothelial-cadherin modulates endothelial monolayer permeability. *J. Cell Sci.* 112:1915–1923.

Hu, X., S. Gan, G. Xie, L. Li, C. Chen, X. Ding, M. Han, S. Xiang, and J. Zhang. 2014. KCTD10 is critical for heart and blood vessel development of zebrafish. *Acta Biochim. Biophys. Sin. (Shanghai).* 46:377–386. https://doi.org/10.1093/abbs/gmu017

Jin, Z., Y. Li, R. Pitti, D. Lawrence, V.C. Pham, J.R. Lill, and A. Ashkenazi. 2009. Cullin3-based polyubiquitination and p62-dependent aggregation of caspase-8 mediate extrinsic apoptosis signaling. *Cell.* 137:721–735. https://doi.org/10.1016/j.cell.2009.03.015

Kroon, J., S. Tol, S. van Amstel, J.A. Elias, and M. Fernandez-Borja. 2013. The small GTPase RhoB regulates TNFα signaling in endothelial cells. *PLoS One.* 8:e75031. https://doi.org/10.1371/journal.pone.0075031

Lebowitz, P.F., J.P. Davide, and G.C. Prendergast. 1995. Evidence that farnesyltransferase inhibitors suppress Ras transformation by interfering with Rho activity. *Mol. Cell. Biol.* 15:6613–6622. https://doi.org/10.1128/MCB.15.12.6613

Lebowitz, P.F., W. Du, and G.C. Prendergast. 1997. Prenylation of RhoB is required for its cell transforming function but not its ability to activate serum response element-dependent transcription. *J. Biol. Chem.* 272:16093–16095. https://doi.org/10.1074/jbc.272.26.16093

Lerm, M., M. Pop, G. Fritz, K. Aktories, and G. Schmidt. 2002. Proteasomal degradation of cytotoxic necrotizing factor 1-activated rac. *Infect. Immun.* 70:4053–4058. https://doi.org/10.1128/IAI.70.8.4053-4058.2002

Liu, A., W. Du, J.P. Liu, T.M. Jessell, and G.C. Prendergast. 2000. RhoB alteration is necessary for apoptotic and antineoplastic responses to farnesyltransferase inhibitors. *Mol. Cell. Biol.* 20:6105–6113. https://doi.org/10.1128/MCB.20.16.6105-6113.2000

Mandik-Nayak, L., J.B. DuHadaway, J. Mulgrew, E. Pigott, K. Manley, S. Sedano, G.C. Prendergast, and L.D. Laury-Kleintop. 2017. RhoB blockade selectively inhibits autoantibody production in autoimmune models of rheumatoid arthritis and lupus. *Dis. Model. Mech.* 10:1313–1322. https://doi.org/10.1242/dmm.029835

Marcos-Ramiro, B., D. García-Weber, S. Barroso, J. Feito, M.C. Ortega, E. Cernuda-Morollón, N. Reglero-Real, L. Fernández-Martín, M.C. Durán, M.A. Alonso, et al. 2016. RhoB controls endothelial barrier recovery by inhibiting Rac1 trafficking to the cell border. *J. Cell Biol.* 213:385–402. https://doi.org/10.1083/jcb.201504038

McNair, K., R. Spike, C. Guilding, G.C. Prendergast, T.W. Stone, S.R. Cobb, and B.J. Morris. 2010. A role for RhoB in synaptic plasticity and the regulation of neuronal morphology. *J. Neurosci.* 30:3508–3517. https://doi.org/10.1523/JNEUROSCI.5386-09.2010

Michaelson, D., J. Silletti, G. Murphy, P. D'Eustachio, M. Rush, and M.R. Philips. 2001. Differential localization of Rho GTPases in live cells: Regulation by hypervariable regions and RhoGDI binding. *J. Cell Biol.* 152:111–126. https://doi.org/10.1083/jcb.152.1.111

Nathan, J.A., H.T. Kim, L. Ting, S.P. Gygi, and A.L. Goldberg. 2013. Why do cellular proteins linked to K63-polyubiquitin chains not associate with proteasomes? *EMBO J.* 32:552–565. https://doi.org/10.1038/emboj.2012.354

Neel, N.F., L.A. Lapierre, J.R. Goldenring, and A. Richmond. 2007. RhoB plays an essential role in CXCR2 sorting decisions. *J. Cell Sci.* 120:1559–1571. https://doi.org/10.1242/jcs.03437

Nethe, M., and P.L. Hordijk. 2010. The role of ubiquitylation and degradation in RhoGTPase signalling. *J. Cell Sci.* 123:4011–4018. https://doi.org/10.1242/jcs.078360

Nethe, M., E.C. Anthony, M. Fernandez-Borja, R. Dee, D. Geerts, P.J. Hensbergen, A.M. Deelder, G. Schmidt, and P.L. Hordijk. 2010. Focal-adhesion targeting links caveolin-1 to a Rac1-degradation pathway. *J. Cell Sci.* 123:1948–1958. https://doi.org/10.1242/jcs.062919

Nobes, C.D., and A. Hall. 1995. Rho, rac, and cdc42 GTPases regulate the assembly of multimolecular focal complexes associated with actin stress fibers, lamellipodia, and filopodia. *Cell.* 81:53–62. https://doi.org/10.1016/0092-8674(95)90370-4

Oberoi, T.K., T. Dogan, J.C. Hocking, R.P. Scholz, J. Mooz, C.L. Anderson, C. Karreman, D. Meyer zu Heringdorf, G. Schmidt, M. Ruonala, et al. 2012. IAPs regulate the plasticity of cell migration by directly targeting Rac1 for degradation. *EMBO J.* 31:14–28. https://doi.org/10.1038/emboj.2011.423

Ozaki, H., T. Hla, and M.J. Lee. 2003. Sphingosine-1-phosphate signaling in endothelial activation. *J. Atheroscler. Thromb.* 10:125–131. https://doi.org/10.5551/jat.10.125

Pierce, R.W., J. Merola, J.P. Lavik, M.S. Kluger, A. Huttner, M.K. Khokha, and J.S. Pober. 2017. A p190BRhoGAP mutation and prolonged RhoB activation in fatal systemic capillary leak syndrome. *J. Exp. Med.* 214:3497–3505. https://doi.org/10.1084/jem.20162143

Pintard, L., A. Willems, and M. Peter. 2004. Cullin-based ubiquitin ligases: Cul3-BTB complexes join the family. *EMBO J.* 23:1681–1687. https://doi.org/10.1038/sj.emboj.7600186

Prendergast, G.C. 2001. Actin' up: RhoB in cancer and apoptosis. *Nat. Rev. Cancer.* 1:162–168. https://doi.org/10.1038/35101096

Pronk, M.C.A., J.S.M. van Bezu, G.P. van Nieuw Amerongen, V.W.M. van Hinsbergh, and P.L. Hordijk. 2017. RhoA, RhoB and RhoC differentially regulate endothelial barrier function. *Small GTPases.* https://doi.org/10.1080/21541248.2017.1339767

Reinhard, N.R., S.F. van Helden, E.C. Anthony, T. Yin, Y.I. Wu, J. Goedhart, T.W. Gadella, and P.L. Hordijk. 2016. Spatiotemporal analysis of RhoA/B/C activation in primary human endothelial cells. *Sci. Rep.* 6:25502. https://doi.org/10.1038/srep25502

Ren, K., J. Yuan, M. Yang, X. Gao, X. Ding, J. Zhou, X. Hu, J. Cao, X. Deng, S. Xiang, and J. Zhang. 2014. KCTD10 is involved in the cardiovascular system and Notch signaling during early embryonic development. *PLoS One.* 9:e112275. https://doi.org/10.1371/journal.pone.0112275

Ridley, A.J., and A. Hall. 1992. The small GTP-binding protein rho regulates the assembly of focal adhesions and actin stress fibers in response to growth factors. *Cell.* 70:389–399. https://doi.org/10.1016/0092-8674(92)90163-7

Ridley, A.J., H.F. Paterson, C.L. Johnston, D. Diekmann, and A. Hall. 1992. The small GTP-binding protein rac regulates growth factor-induced membrane ruffling. *Cell.* 70:401–410. https://doi.org/10.1016/0092-8674(92)90164-8

Sakaue, T., A. Fujisaki, H. Nakayama, M. Maekawa, H. Hiyoshi, E. Kubota, T. Joh, H. Izutani, and S. Higashiyama. 2017a. Neddylated Cullin 3 is required for vascular endothelial-cadherin-mediated endothelial barrier function. *Cancer Sci.* 108:208–215. https://doi.org/10.1111/cas.13133

Sakaue, T., I. Sakakibara, T. Uesugi, A. Fujisaki, K.I. Nakashiro, H. Hamakawa, E. Kubota, T. Joh, Y.K. Imai, H. Izutani, and S. Higashiyama. 2017b. The CUL3-SPOP-DAXX axis is a novel regulator of VEGFR2 expression in vascular endothelial cells. *Sci. Rep.* 7:42845. https://doi.org/10.1038/srep42845

Schaefer, A., N.R. Reinhard, and P.L. Hordijk. 2014. Toward understanding RhoGTPase specificity: structure, function and local activation. *Small GTPases.* 5:6. https://doi.org/10.4161/21541248.2014.968004

Soucy, T.A., P.G. Smith, M.A. Milhollen, A.J. Berger, J.M. Gavin, S. Adhikari, J.E. Brownell, K.E. Burke, D.P. Cardin, S. Critchley, et al. 2009. An inhibitor of NEDD8-activating enzyme as a new approach to treat cancer. *Nature.* 458:732–736. https://doi.org/10.1038/nature07884

Timmerman, I., N. Heemskerk, J. Kroon, A. Schaefer, J. van Rijssel, M. Hoogenboezem, J. van Unen, J. Goedhart, T.W. Gadella Jr., T. Yin, et al. 2015. A local VE-cadherin and Trio-based signaling complex stabilizes endothelial junctions through Rac1. *J. Cell Sci.* 128:3041–3054. https://doi.org/10.1242/jcs.168674

Tong, X., Y. Zu, Z. Li, W. Li, L. Ying, J. Yang, X. Wang, S. He, D. Liu, Z. Zhu, et al. 2014. Kctd10 regulates heart morphogenesis by repressing the transcriptional activity of Tbx5a in zebrafish. *Nat. Commun.* 5:3153. https://doi.org/10.1038/ncomms4153

Torrino, S., O. Visvikis, A. Doye, L. Boyer, C. Stefani, P. Munro, J. Bertoglio, G. Gacon, A. Mettouchi, and E. Lemichez. 2011. The E3 ubiquitin-ligase HACE1 catalyzes the ubiquitylation of active Rac1. *Dev. Cell.* 21:959–965. https://doi.org/10.1016/j.devcel.2011.08.015

van Nieuw Amerongen, G.P., S. van Delft, M.A. Vermeer, J.G. Collard, and V.W. van Hinsbergh. 2000. Activation of RhoA by thrombin in endothelial hyperpermeability: role of Rho kinase and protein tyrosine kinases. *Circ. Res.* 87:335–340. https://doi.org/10.1161/01.RES.87.4.335

van Nieuw Amerongen, G.P., C.M. Beckers, I.D. Achekar, S. Zeeman, R.J. Musters, and V.W. van Hinsbergh. 2007. Involvement of Rho kinase in endothelial barrier maintenance. *Arterioscler. Thromb. Vasc. Biol.* 27:2332–2339. https://doi.org/10.1161/ATVBAHA.107.152322

Verin, A.D., A. Birukova, P. Wang, F. Liu, P. Becker, K. Birukov, and J.G. Garcia. 2001. Microtubule disassembly increases endothelial cell barrier dysfunction: role of MLC phosphorylation. *Am. J. Physiol. Lung Cell. Mol. Physiol.* 281:L565–L574. https://doi.org/10.1152/ajplung.2001.281.3.L565

Vouret-Craviari, V., C. Bourcier, E. Boulter, and E. van Obberghen-Schilling. 2002. Distinct signals via Rho GTPases and Src drive shape changes by thrombin and sphingosine-1-phosphate in endothelial cells. *J. Cell Sci.* 115:2475–2484.

Wang, H.R., A.A. Ogunjimi, Y. Zhang, B. Ozdamar, R. Bose, and J.L. Wrana. 2006. Degradation of RhoA by Smurf1 ubiquitin ligase. *Methods Enzymol.* 406:437–447. https://doi.org/10.1016/S0076-6879(06)06032-0

Wherlock, M., A. Gampel, C. Futter, and H. Mellor. 2004. Farnesyltransferase inhibitors disrupt EGF receptor traffic through modulation of the RhoB GTPase. *J. Cell Sci.* 117:3221–3231. https://doi.org/10.1242/jcs.01193

Wojciak-Stothard, B., L. Zhao, E. Oliver, O. Dubois, Y. Wu, D. Kardassis, E. Vasilaki, M. Huang, J.A. Mitchell, L.S. Harrington, et al. 2012. Role of RhoB in the regulation of pulmonary endothelial and smooth muscle cell responses to hypoxia. *Circ. Res.* 110:1423–1434. https://doi.org/10.1161/CIRCRESAHA.112.264473

Xu, J., L. Li, G. Yu, W. Ying, Q. Gao, W. Zhang, X. Li, C. Ding, Y. Jiang, D. Wei, et al. 2015. The neddylation-cullin 2-RBX1 E3 ligase axis targets tumor suppressor RhoB for degradation in liver cancer. *Mol. Cell. Proteomics.* 14:499–509. https://doi.org/10.1074/mcp.M114.045211

Yang, Y., Y. Ma, C. Shi, H. Chen, H. Zhang, N. Chen, P. Zhang, F. Wang, J. Yang, J. Yang, et al. 2013a. Overexpression of miR-21 in patients with ulcerative colitis impairs intestinal epithelial barrier function through targeting the Rho GTPase RhoB. *Biochem. Biophys. Res. Commun.* 434:746–752. https://doi.org/10.1016/j.bbrc.2013.03.122

Yang, Y., L. Sun, L. Tala, D. Gao, J. Li, Zhou, and M. Liu. 2013b. CYLD regulates RhoA activity by modulating LARG ubiquitination. *PLoS One.* 8:e55833. https://doi.org/10.1371/journal.pone.0055833

Yuan, W.C., Y.R. Lee, S.Y. Lin, L.Y. Chang, Y.P. Tan, C.C. Hung, J.C. Kuo, C.H. Liu, M.Y. Lin, M. Xu, et al. 2014. K33-Linked Polyubiquitination of Coronin 7 by Cul3-KLHL20 Ubiquitin E3 Ligase Regulates Protein Trafficking. *Mol. Cell.* 54:586–600. https://doi.org/10.1016/j.molcel.2014.03.035

Zhang, W., and S.S. Sidhu. 2014. Development of inhibitors in the ubiquitination cascade. *FEBS Lett.* 588:356–367. https://doi.org/10.1016/j.febslet.2013.11.003

Zhao, J., R.K. Mialki, J. Wei, T.A. Coon, C. Zou, B.B. Chen, R.K. Mallampalli, and Y. Zhao. 2013. SCF E3 ligase F-box protein complex SCF(FBXL19) regulates cell migration by mediating Rac1 ubiquitination and degradation. *FASEB J.* 27:2611–2619. https://doi.org/10.1096/fj.12-223099